ACS OMEGA

http://pubs.acs.org/journal/acsodf

Article

Photochemical and Photobiological Properties of Pyridyl-pyrazol(in)e-Based Ruthenium(II) Complexes with Sub-micromolar Cytotoxicity for Phototherapy

Dmytro Havrylyuk,* David K. Heidary, Yang Sun, Sean Parkin, and Edith C. Glazer*

Cite This: https://dx.doi.org/10.1021/acsomega.0c02079

Read Online

ACCESS | Metrics & More | Article Recommendations | Supporting Information

ABSTRACT: The discovery of new light-triggered prodrugs based on ruthenium (II) complexes is a promising approach for photoactivated chemotherapy (PACT). The light-mediated activation of "strained" Ru(II) polypyridyl complexes resulted in ligand release and produced a ligand-deficient metal center capable of forming covalent adducts with biomolecules such as DNA. Based on the strategy of exploiting structural distortion to activate photochemistry, biologically active small molecules were coordinated to a Ru(II) scaffold to create light-triggered dual-action agents. Thirteen new Ru(II) complexes with pyridyl-pyrazol(in)e ligands were synthesized, and their photochemical reactivity and anticancer properties were investigated. Isomeric bidentate ligands were investigated, where "regular" ligands (where the coordinated nitrogens in the heterocycles are linked by C−C atoms) were compared to "inverse" isomers (where the coordinated nitrogens in the heterocycles are linked by C−N atoms). Coordination of the regular 3-(pyrid-2-yl)-pyrazol(in)es to a Ru(II) bis-dimethylphenanthroline scaffold yielded photoresponsive compounds with promising photochemical and biological properties, in contrast to the inverse 1-(pyrid-2-yl)-pyrazolines. The introduction of a phenyl ring to the 1*N*-pyrazoline cycle increased the distortion in complexes and improved ligand release upon light irradiation (470 nm) up to 5-fold in aqueous media. Compounds **1**−**8**, containing pyridyl-pyrazol(in)e ligands, were at least 20−80-fold more potent than the parent pyridyl-pyrazol(in)es, and exhibited biological activity in the dark, with half-maximal inhibitory concentration (IC_{50}) values ranging from 0.2 to 7.6 μM in the HL60 cell line, with complete growth inhibition upon light irradiation. The diversification of coligands and introduction of a carboxylic acid into the Ru(II) complex resulted in compounds **9**−**12**, with up to 146-fold improved phototoxicity indices compared with complexes **1**−**8**.

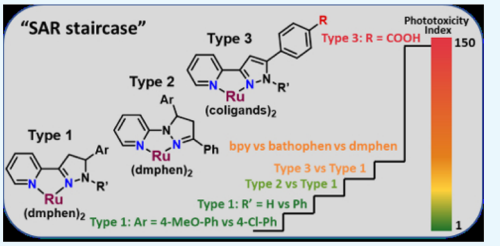

1. INTRODUCTION

The investigation of new ruthenium-based compounds as alternatives to anticancer platinum drugs is a developing trend in modern medicinal inorganic chemistry.[1−6] Based on the specific chemical features of ruthenium complexes, drug discovery efforts can be divided into two categories: (1) development of agents which are prone to ligand exchange (for example, NAMI-A and KP1339, which were in phase II clinical trials, and RAPTA-C, which is progressing toward clinical trials),[7−10] and (2) investigation of kinetically inert ruthenium-(II) polypyridyl complexes as either agents possessing anticancer potency without irradiation[11−13] or prodrugs for photodynamic therapy (PDT; for example, TLD1433, now in phase II clinical trials) and photoactivated chemotherapy (PACT).[2,6,14−16]

The structural and functional diversification of bidentate ligands incorporated into octahedral ruthenium complexes has a crucial impact on both the photochemical features and the anticancer potency of compounds. The chemical modification of heteroleptic light-activated ruthenium-based prodrugs with bidentate ligands is usually focused on the optimization of polypyridine-type compounds[14,17−22] or in some cases *S*-coordinating ligands.[23,24] Recently, we investigated a class of bidentate ligands containing different five-membered ring heterocycles (indole, benzimidazole, benzoxazole, and benzothiazole).[16] Using these systems, Ru(II) complexes were developed that rapidly release ligands in aqueous (aq) solutions, forming biologically active photoproducts. The compounds were highly effective in killing leukemic cells when irradiated, but the high toxicity of the compounds in the dark could be a limitation for their potential application as PACT agents.[16] To continue the investigation of heteroleptic ruthenium complexes based on five-membered heterocycles, the purpose of this project was the coordination of pyridyl-pyrazoline (pyrazoline = 4,5-dihydropyrazole) and pyridyl-pyrazole ligands to Ru(II) scaffolds, aiming to identify new promising anticancer agents with potential for PDT or PACT.

Pyrazole and pyrazoline are important heterocycles contained in many bioactive agents that display a broad spectrum

Received: May 5, 2020
Accepted: July 10, 2020

Chart 1. Small Molecules with Pyrazole (Red) and Pyrazoline (Blue) Scaffolds (I–V) and Metal Complexes Containing Pyrazol(in)e Ligands (VI–XI) That Exhibit Anticancer Activity[a]

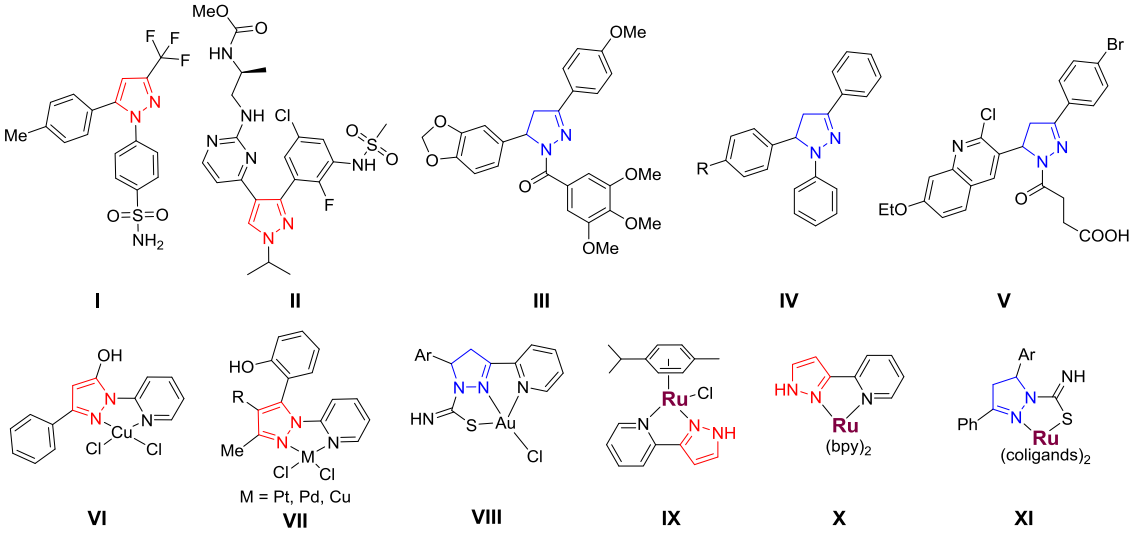

[a]Ru atoms are colored purple. The structures **VI** and **VII** contain C–N linkages (inverse ligands) and the structures **VIII–X** contain C–C linkages (regular ligands).

of biological activities, including antitumor properties.[25] For example, celecoxib (a nonsteroidal anti-inflammatory drug, compound **I**, Chart 1) has shown promise in the prevention of cancer and has been used to reduce the number of adenomatous colorectal polyps in patients with the hereditary colon cancer susceptibility syndrome.[26] Recently, encorafenib (**II**) has been approved for combination therapy for patients with unresectable or metastatic melanoma with a BRAF V600E or V600K mutation.[27] The cytotoxic mechanisms of 3,5-diarylsubstituted pyrazolines have been associated with their inhibition of tubulin polymerization (compound **III**),[28] mammalian cathepsin B and H (compounds **IV**),[29] and replication protein A (compound **V**).[30] Recently, one of us explored the hybridization of pyrazoline scaffold with other heterocycles (thiazolidine, indoline) as a direction for the enhancement of their biological properties. These pyrazoline-based conjugates possessed promising anticancer,[31−36] antiviral,[32] and antitrypanosomal[37] activities in vitro. It is also known that the coordination of pyrazoles and pyrazolines to different metal centers is a successful approach to increase their anticancer activity. The cytotoxic effects of Pt(II),[38] Pd(II),[38] Cu(II),[38,39] and Au(III)[40] complexes (**VI–VIII**) with pyridyl-pyrazol(in)e ligands have been reported recently, with activity at micromolar concentrations. Ru(II) complexes with pyridyl-pyrazole ligand have been reported, and the arene complex **IX** exhibited selective cytotoxic activity against breast cancer cells in vitro.[41] Complex **X** possessed light-mediated anticancer activity both in vitro and in vivo and has been identified as a potential candidate for PDT.[42] Notably, the pyrazoline-thioamides coordinated to Ru(II) scaffolds **XI** possessed cytotoxic activity at sub-micromolar concentration (Chart 1).[43]

Coordination of ruthenium scaffolds containing ortho-substituted phenanthroline-type ligands ($[Ru(dmphen)_2]^{2+}$; dmphen is 2,9-dimethyl-1,10-phenanthroline) led to the identification of complexes with cytotoxicity toward cancer cells at micromolar concentrations.[44−59] This scaffold exhibits an intrinsically distorted octahedral geometry, and when explored for PDT or PACT applications, some of the complexes exhibited sub-micromolar anticancer activity via light-mediated ligand release and covalent binding to DNA.[16,17,60] In addition to steric factors, electronic features also can modulate photochemistry, and we have previously explored this through incorporation of additional nitrogens within coordinating heterocycles.[61,62] Moreover, the placement of biaryl linkages in pyridyl triazoles, either at the regular position, between two carbons, or the inverse position, between a carbon and a nitrogen of the triazole, has been demonstrated to regulate the photochemistry of Ru(II) complexes.[63,64] To test this strategy, we investigated analogous regular and inverse pyrazol(in)es, which we name by the same convention. Here, we report the design and synthesis of new $[Ru(dmphen)_2]^{2+}$ complexes based on regular 3-(pyrid-2-yl)-pyrazol(in)es (types 1 and 3, Chart 2) and inverse 1-(pyrid-2-yl)-pyrazolines (type 2), their photochemical properties in aqueous media, their in vitro anticancer activity, and the structure–activity relationships (SARs) that emerged for the tested compounds.

Chart 2. Ru(II) Complexes (1–12) with the Regular Pyridyl-pyrazolines (Type 1), Inverse Pyridyl-pyrazolines (Type 2), and Regular Pyridyl-pyrazoles (Type 3)

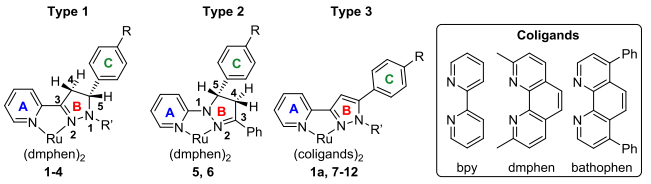

We have discovered that distorted heteroleptic Ru(II) complexes with pyridyl-pyrazol(in)e ligands are photoreactive and exhibited selective photoejection of the pyrazole-containing ligand when irradiated with blue light. Their photochemical properties and anticancer profile depended significantly on the type of pyrazol(in)e ligand (regular vs inverse). The coordination of inactive regular pyridyl-pyrazol(in)es to the Ru(II) scaffold resulted in compounds with sub-micromolar cytotoxicity without irradiation. This finding could

https://dx.doi.org/10.1021/acsomega.0c02079
ACS Omega XXXX, XXX, XXX−XXX

be useful for further investigation of the complexes as traditional anticancer agents but precludes their application for PACT. Similarly, the inverse pyridyl-pyrazol(in)es were potent in the dark but were not light-active cytotoxins. However, the addition of the substituents to the aryl group appended to the 5-position of the five-membered ring heterocycle (cycle C, Chart 2) altered the key properties and rendered the regular pyridyl-pyrazol(in)es useful as PACT agents. Based on a rationale design theory, the inclusion of a carboxylic group into the pyridyl-pyrazole ligand (compound **11**) radically reduced the dark cytotoxicity of Ru(II) complexes while simultaneously increasing the phototoxicity index (PI = 146). Considering the significant anticancer potential of pyrazol(in)e-based hybrids,[25] these findings could be useful for the improvement of similar small-molecules' cytotoxicity by coordination to the Ru(II) center, and/or further investigation of the potential light-activated, dual-action cytotoxic agents.

2. RESULTS AND DISCUSSION

2.1. Chemistry. The regular 3-(pyrid-2-yl)-4,5-dihydropyrazoles were synthesized from 2-acetylpyridine via a Claisen−Schmidt condensation with aromatic aldehydes, followed by heterocyclization of chalcones to pyrazolines with hydrazine hydrate[65] or phenylhydrazine.[66] To expand the structure−activity relationships, we carried out the oxidation of the pyrazolines to pyrazoles[67] and synthesized the inverse 1-(pyrid-2-yl)-pyrazoline ligands[68] (Scheme S1). The Ru(II) complexes **1**−**12** (Chart 3) were synthesized from a racemic mixture of the Δ and Λ enantiomers of the Ru(II) starting materials, and form a mixture of enantiomers upon coordination of the pyridyl-pyrazol(in)e ligands. Compounds **1**−**8** and **11** were synthesized from $Ru(dmphen)_2Cl_2$, compound **9** from $Ru(bpy)_2Cl_2$ (bpy is 2,2′-bipyridine), and compounds **10** and **12** from $Ru(bathophen)_2Cl_2$ (bathophen is 4,7-diphenyl-1,10-phenanthroline). The purity of all compounds was determined by high-performance liquid chromatography (HPLC) (detection wavelength = 280 nm; Figures S33−S35). The Ru(II) complexes containing pyridyl-pyrazoline ligands (**1**−**6**) may exist as a mixture of four stereoisomers owing to the presence of two chiral centers (Figure S1), i.e., metal (Λ/Δ) and ligand (*R*/*S*). The ^{1}H NMR spectra of **1**−**6** exhibited the characteristic patterns of two AMX systems for CH_2−CH protons of the pyrazoline fragment and evidenced the presence of diastereomers in the racemic mixture. In contrast to compounds **3** and **4**, there is no preference of one diastereomer for compounds **5** and **6**. Interestingly, the HPLC chromatograms for **5** and **6** exhibited two peaks with similar UV/vis profiles (Figure S33), indicating the separation of different diastereomers under HPLC conditions.

Upon coordination of the 3-(pyrid-2-yl)-pyrazoline ligand (L1, Scheme S1) to $[Ru(dmphen)_2]$, the oxidation of the pyrazoline cycle into pyrazole was observed. The oxidized product **1a** was isolated and fully characterized by NMR, electrospray ionization mass spectrometry (ESI MS), and X-ray. Apparently, compound **1a** may exist as an impurity of compound **1**, and the oxidation of the pyrazoline cycle may occur not only under reaction conditions, but also upon storage when not protected from air. To minimize the impact of oxidation on compounds **1** and **2**, rapid characterization was conducted by ESI MS and ^{1}H NMR techniques. Compound **1** (as the PF_6 salt) exhibited a $[M]^{2+}$ ion at *m*/*z* 385.6 in the ESI MS spectrum. In contrast, the $[M]^{2+}$ ion for compound **1a** was detected at *m*/*z* 384.4 (Figures S36 and S37). The ^{1}H NMR spectrum of **1** showed a minor impurity of oxidized form, but the HPLC trace of compound **1** (with Cl^- counterions) exhibited two peaks (Figure S34). While the oxidation of compounds **1** and **2** under air condition is a significant disadvantage for their in-depth investigation and their potential advancement, we decided to include them for the studies reported below to determine if these structures were worth further efforts.

Chart 3. Structures of Complexes Included in This Study[a]

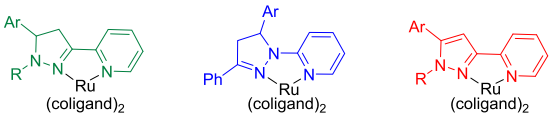

Compound	Coligand	Pyridyl-pyrazol(in)e ligand
1	dmphen	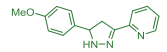
1a	dmphen	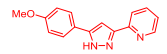
2	dmphen	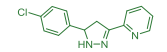
3	dmphen	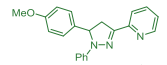
4	dmphen	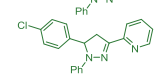
5	dmphen	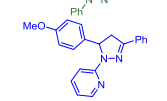
6	dmphen	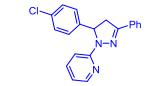
7	dmphen	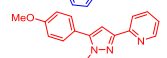
8	dmphen	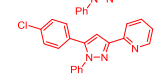
9	bpy	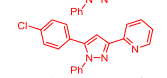
10	bathophen	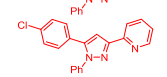
11	dmphen	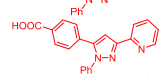
12	bathophen	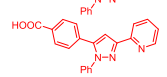

[a]The regular pyridyl-pyrazoline (green), inverse pyridyl-pyrazoline (blue), and pyridyl-pyrazole (red) ligands were combined with the indicated coligands to make bis heteroleptic Ru(II) complexes.

2.2. Crystallography. The structures of three complexes containing bidentate pyridyl-pyrazoline or pyrazole ligands, **1a**, **4**, and **8**, were determined by X-ray crystallography and are contrasted in Figures 1 and S2−S5. Selected bond lengths and angles are listed in Table 1.

All three complexes exhibited a distorted octahedral geometry due to the incorporation of two dmphen ligands. This resulted in the Ru−N(dmphen) bond lengthening to 2.100 Å (average value for **1a**), 2.122 Å (average value for **4**), and 2.115 Å (average value for **8**) in comparison with 2.06 Å for analogous complexes with 2,2′-bipyridyl (bpy) coligands.[69] The average bond length of Ru−N5 and Ru−N6 for complex **4** is about 2.07 Å, which is almost the same as that of the $[Ru(bpy)_2]^{2+}$ analogous complex and $[Ru(bpy)_3]^{2+}$.[70] However, the average bond lengths for the pyridyl-pyrazole Ru−N5

https://dx.doi.org/10.1021/acsomega.0c02079
ACS Omega XXXX, XXX, XXX−XXX

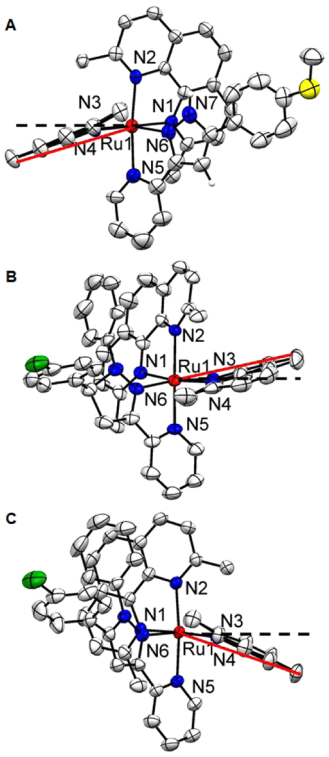

Figure 1. Ellipsoid plot of ruthenium complexes **1a** (A), **4** (B), and **8** (C) at 50% probability with H atoms omitted for clarity. These side views highlight the distortion of the dmphen ligand. The black dashed line indicates the plane defined by the N3−Ru−N4 atoms, and the angle between red and black dash lines represents the ligand bend.

Table 1. Selected Bond Lengths (Å) and Bond Angles (deg) of 1a, 4, and 8

	1a	4	8
	Bond Lengths (Å)		
Ru−N1	2.117(3)	2.124(4)	2.114(2)
Ru−N2	2.094(3)	2.130(4)	2.108(2)
Ru−N3	2.084(3)	2.112(4)	2.102(2)
Ru−N4	2.103(3)	2.121(4)	2.134(2)
Ru−N5	2.109(4)	2.070(4)	2.108(2)
Ru−N6	2.117(3)	2.075(4)	2.123(2)
	Bond Angles (deg)		
N1−Ru−N2	79.42(12)	79.14(15)	79.38(10)
N1−Ru−N3	102.41(12)	93.16(16)	100.63(9)
N1−Ru−N4	177.93(12)	170.29(17)	177.01(9)
N1−Ru−N5	96. 34(13)	102.15(16)	97. 5(1)
N1−Ru−N6	80.45(12)	86.54(16)	83.5(1)
N2−Ru−N3	93.81(12)	85.41(15)	92.99(9)
N2−Ru−N4	100.94(12)	93.59(15)	103.6(1)
N2−Ru−N5	173.62(13)	178.71(15)	174.12(9)
N2−Ru−N6	96.87(13)	102.33(15)	96.66(9)
N3−Ru−N4	79.62(12)	79.74(18)	79.42(9)
N3−Ru−N5	91.76(13)	94.44(16)	92.49(10)
N3−Ru−N6	169.30(13)	172.04(15)	170.07(9)
N4−Ru−N5	83.12(13)	85.13(16)	79.52(9)
N4−Ru−N6	97.48(13)	101.41(17)	95.98(9)
N5−Ru−N6	77.63(14)	77.86(16)	77.97(10)
dmphen (N1−N2) bend[a]	21.88	−11.0	16.89
dmphen (N3−N4) bend[b]	19.58	−10.64	22.06

[a]Average angle (N3−Ru−C13/C14)—90°. [b]Average angle (N2−Ru−C27/C28)—90°.

and Ru−N6 for complexes **1a** (2.113 Å) and **8** (2.116 Å) are equal to the length of Ru−N(dmphen) bonds and are longer than the analogous bonds for the pyridyl-pyrazoline ligand in complex **4** (Table 1) and the dipyridylphenazine ligand (dppz, 2.083 Å) coordinated to the $[Ru(dmphen)_2]$ scaffold.[71]

The bond angles between the trans-nitrogens of the two dmphen ligands (N1 and N4) are nonequivalent, with nearly a 10° deviation from the ideal 180° angle for complexes **1a** and **4** (Table 1). Both dmphen ligands (Figure 1 and Table 1) for compounds **1a**, **4**, and **8** are considerably bent from the normal plane, exhibiting misdirected metal−ligand bonds.[72] In addition, the directions of the dmphen bends are different. The dmphen ligand (N3−N4) is bent toward dmphen (N1−N2) for compound **4**, while, in contrast, the dmphen ligand (N3−N4) bend for **1a** and **8** is directed toward the pyridyl-pyrazole ligand (Figure 1). The significant distortion from the ideal octahedral geometry reflects the strain in the molecules. The nonequivalent bends of the dmphen ligands could cause a difference in the photoejection kinetics for Ru(II) complexes with pyridyl-pyrazoline and pyridyl-pyrazole ligands.

2.3. Photochemistry. The strained Ru(II) complexes **1**−**8** and **11** all exhibited selective photoejection of the pyridyl-pyrazole or pyridyl-pyrazoline ligand when irradiated with 470 nm light, as shown in Figures 2 and S6−S14. The photochemical reactions were monitored by absorption spectroscopy, and the presence of an isosbestic point indicated the direct conversion to a single product (Figure 2A). The selective ejection of the pyridyl-pyrazoline/pyrazole ligands after irradiation of **4** and **8** in water was confirmed by HPLC through comparison with the starting complexes and ligands (Figure 2C,D). No dmphen was ejected under these conditions, excluding the possibility of the cytotoxic effect of dmphen in the cellular assay.[73] The UV/vis spectra upon irradiation of **1**−**8** and **11** in water exhibited the absorbance peak at 495 nm (Figures 1B and S6−S14) corresponding to the $[Ru(dmphen)_2(H_2O)_2]^{2+}$ photoproduct.[74] The photosubstitution quantum yields (Φ_{PS}) for the complexes **1**−**8** and **11** with the Cl counterions were determined by an optical approach, as has been described previously.[61] Φ_{PS} values for complexes **3**, **4**, **7**, and **8** were found to be up to 5-fold higher than for compounds **1** and **2**. This variation in the photochemical reactivity suggests that introduction of a phenyl ring at the 1*N* of pyrazoline/pyrazole ligands increases the strain in the molecules (**3**, **4**, **7**, and **8**) and improves the photochemical reactivity. Ru(II) complexes **5** and **6** with inverse ligands exhibited 2−4-fold lower Φ_{PS} values than isomeric compounds **3** and **4** in both water and Opti-MEM. Considering that the same steric effect of the phenyl ring exists for both the regular and inverse pyridyl-ligand, the disparity in photoejection kinetics can potentially be explained by the different pK_a values for bidentate ligands (Chart S1). The regular system has a lower pK_a, which we have previously shown is associated with higher Φ_{PS} values.[61] Notably, the replacement of the electron-donating methoxy group (**1**, **3**, **5**, and **7**) with an electron-withdrawing chlorine (**2**, **4**, **6**, and **8**) had a minor effect on photoreactivity.

2.4. DNA Damage. Due to the rapid photochemistry of the regular 3-(pyrid-2-yl)-1*N*-phenyl-pyrazol(in)e ligands in aqueous media, the interaction of compounds **4** and **8** with DNA was studied. DNA damage was assessed by gel electrophoresis using pUC19 plasmid DNA (Figure 3). Incubation of Ru(II) complexes **4** and **8** with plasmid DNA in the dark showed no interactions that caused structural

https://dx.doi.org/10.1021/acsomega.0c02079
ACS Omega XXXX, XXX, XXX−XXX

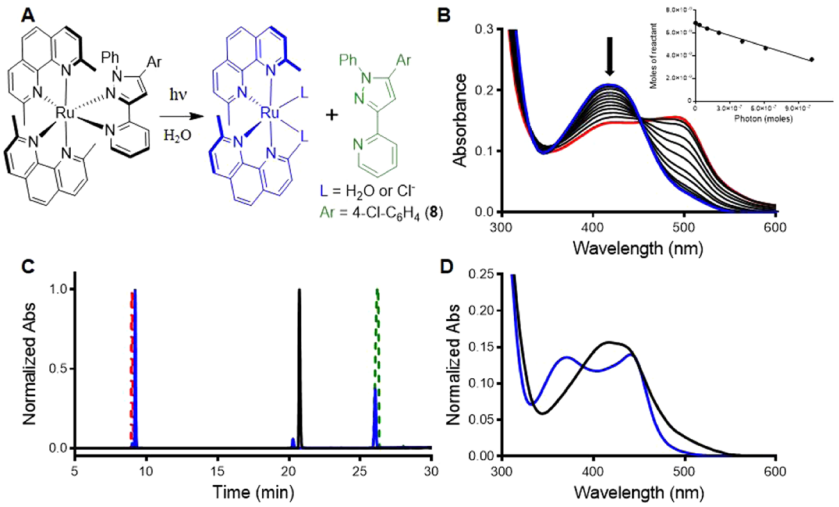

Figure 2. Photochemical reactivity of compound **8**. (A) Photoejection reaction scheme. (B) Photoejection of **8** (30 μM, in water) followed by UV/vis absorption over 0−60 min irradiation with 470 nm light. Inset: linear regression for moles of reactant vs moles of photons absorbed for complex **8**. (C) Determination of the photoejection products by HPLC. Chromatogram of **8** before (black) and after 30 min irradiation (blue), in comparison with starting ligands dmphen (red) and pyridyl-pyrazole (green). (D) Absorption profile of **8** (black, retention time = 20.7 min) and the photochemical product $[Ru(dmphen)_2(L)_2]$ (blue, retention time = 9.2 min); note that the presence of CH_3CN in the HPLC experiment changes the absorption profile for the photoproduct.

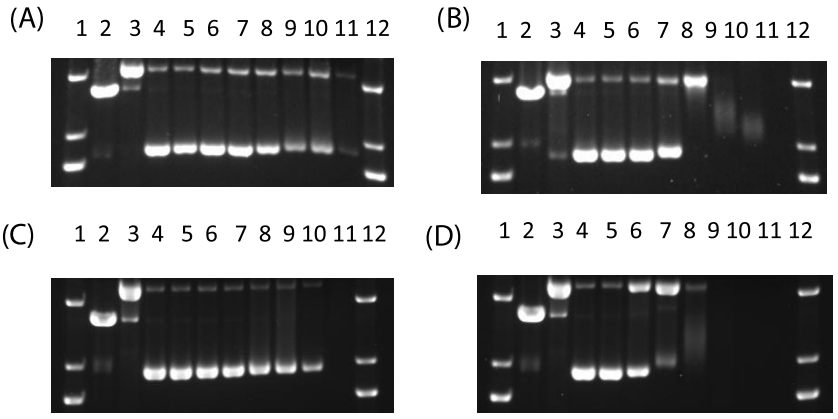

Figure 3. Agarose gel electrophoresis showing the dose response of compounds **4** (A, B) and **8** (C, D) incubated with 40 μg/mL pUC19 DNA in the dark (A, C) and with irradiation (470 nm light, 40 J/cm^2 (B, D)). Lanes 1 and 12, DNA ladder; lane 2, *Eco*RI; lane 3, $Cu(OP)_2$; lane 4−11, 0−500 μM. *Eco*RI and $Cu(OP)_2$ are controls for linear and relaxed circle DNA, respectively.

perturbations at concentrations up to 125 μM (Figure 3A,C). In contrast, two types of DNA damage were observed upon irradiation with 470 nm light (40 J/cm^2). Complexes **4** and **8** undergo ligand loss and covalent attachment to DNA at concentrations above 30 μM, as observed by the reduction of DNA mobility and loss of ethidium bromide (EtBr) staining.[19] The presence of relaxed circular DNA (Figure 3B,D, lanes 6−8) indicated that complexes **4** and **8** also created single-strand breaks.

2.5. Cytotoxicity Studies. The anticancer activity of complexes **1**−**12** was determined against a leukemic cell line (HL60 human promyelocytic leukemia; Table 2). Cell death was determined after 72 h incubation with the complexes in the dark or following a 1 h incubation and subsequent light exposure (29.1 J/cm^2) before the 72 h incubation. The initial SAR study for $[Ru(dmphen)_2]^{2+}$ complexes (**1**−**8**) with the pyridyl-pyrazol(in)e ligands was focused on: (a) the modification of the Ar substituent at the 5-position of the pyrazol(in)e moiety (cycle C, Chart 2); (b) the introduction of a phenyl moiety at the 1*N*-position of pyrazole (R′, see Chart 2); (c) regular and inverse pyridyl-pyrazoline isomerism, and (d) pyrazoline-pyrazole replacement.

Compounds **1**−**4**, **7**, and **8** containing the regular pyridyl-pyrazol(in)e ligands were at least 20−80-fold more potent than the parent pyridyl-pyrazol(in)e ligands (Figures 4A and S15−S19) and exhibited cytotoxicity IC_{50} values ranging from 0.2 to 7.6 μM. The activity of the complexes was sensitive to the modification of the Ar substituent at the 5-position of the pyrazoline moiety (cycle C), the introduction of a phenyl ring at the 1*N*-position (R′ = Ph), or oxidation of the pyrazoline moiety to the aromatic pyrazole (cycle B). The replacement of the electron-donating methoxy group with an electron-withdrawing chlorine had an ambiguous effect. Ruthenium complexes with chloro-substituted pyrazolines (**2**, **4**) exhibited around 2-fold larger anticancer activities than complexes **1** and **3** with the MeO group. However, complex **7** with the *p*-MeO-phenyl-substituted pyrazole ligand was more active than **8**. Despite only small reductions in the cytotoxic properties after introduction of the phenyl ring at the 1*N*-position (compounds **3**, **4**), it should be noted that compounds **1** and **2** (1*NH*-

https://dx.doi.org/10.1021/acsomega.0c02079
ACS Omega XXXX, XXX, XXX−XXX

Table 2. Photophysical and Photochemical Properties, Cytotoxicity Half-Maximal Inhibitory Concentration (IC_{50}) Values (μM, HL60 Cell Line), and Heat Map for the Phototoxicity Indices for Ru(II) Complexes

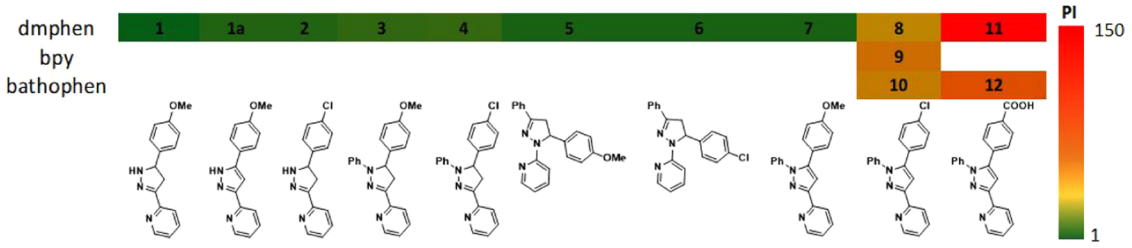

		Φ_{PS}				
compound	λ_{max} (nm)	water	Opti-MEM	dark IC_{50}, μM[a]	light IC_{50}, μM[a]	phototoxicity index, PI[b]
1	445	0.0011(3)	0.0022(4)	1.0 ± 0.1	1.6 ± 0.2	0.6
1a	435	0.0062(4)	0.0034(5)	0.2 ± 0.1	0.2 ± 0.1	1
2	445	0.0009(3)	0.0008(2)	0.6 ± 0.05	0.5 ± 0.05	1.2
3	450	0.0045(5)	0.0051(3)	2.4 ± 0.2	1.5 ± 0.2	1.5
4	450	0.0024(3)	0.0027(5)	0.8 ± 0.2	0.5 ± 0.1	1.6
5	390	0.0014(3)	0.0005(6)	0.8 ± 0.2[c]	1.3 ± 0.2	0.6
6	390	0.0009(3)	0.0016(4)	1.0 ± 0.2[c]	1.4 ± 0.2	0.7
7	415	0.0026(4)	0.0024(5)	0.9 ± 0.1	0.9 ± 0.1	1
8	415	0.0032(6)	0.0028(4)	7.6 ± 0.3	1.5 ± 0.2	5
9	410	n.r.[d]	n.r.	44.7 ± 1.5	1.6 ± 0.3	28
10	425	n.r.	n.r.	8.5 ± 0.2	0.6 ± 0.2	14
11	415	0.0057(4)	0.0061(6)	116.7 ± 6.6	0.8 ± 0.3	146
12	425	n.r.	n.r.	29.3 ± 1.5	0.5 ± 0.2	59

[a]Cytotoxicity of compounds evaluated as the average of three measurements. The IC_{50} value of cisplatin is 3.1 ± 0.3 μM. [b]The phototoxicity index (PI) is the ratio of the dark and light IC_{50} values. [c]Only 60% cell death was achieved at higher concentrations. [d]n.r. = no reaction.

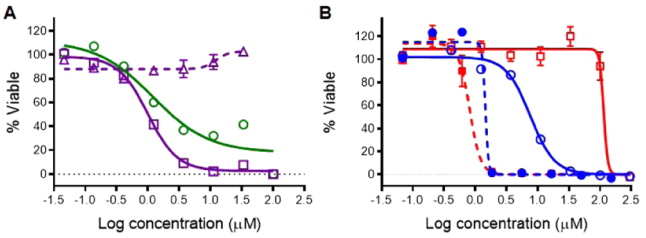

Figure 4. Cytotoxicity dose responses of ruthenium complexes **1**, **3**, **8**, and **11** on the HL60 cells (n = 3): (A) compound **1** (□, solid purple line) in comparison with the parent pyridyl-pyrazoline ligand (Δ, dashed purple line) and complex **3** (○, solid green line); (B) light-mediated cytotoxicity for compounds **8** (○, blue) and **11** (□, red), indicating the improvement in the PI by introduction of a carboxylic acid group into the pyridyl-pyrazole ligand (solid line—dark conditions; dashed line—upon 1 min irradiation with >450 nm light, 29.1 J/cm^2).

pyrazoline derivatives) exhibited total growth inhibition of cancer cells (0% viable cells) at lower concentrations than corresponding *N*-Ph-substituted analogous complexes **3** and **4** (Figure S16). The coordination of inverse pyridyl-pyrazoline ligands (type 2) to the $[Ru(dmphen)_2]^{2+}$ scaffold (complexes **5** and **6**) did not result in significant improvements in anticancer activity compared to isomeric compounds **3** and **4**. Notably, compound **1a** exhibited the highest anticancer activity on the HL60 cell line with an IC_{50} value of 0.2 μM, making it 15-fold more potent than cisplatin.

The photoreactive compounds **1**−**8** were tested for their anticancer activity upon light activation, but except for compound **8**, did not exhibit significant improvements in cytotoxicity upon irradiation (see the phototoxicity index (PI) values in Table 2). However, light activation of **3**−**8** resulted in much steeper dose response curves, achieving essentially complete cell death (0% viable cells) at 10-fold lower concentrations than the same compound in the dark (Figures S16 and S17). This indicates a different mechanisms of action with regards to the cause of the cell death upon irradiation vs the nonirradiated cells.

Considering the low phototoxicity indices for compounds **1**−**8**, the focus shifted to diversification of the coligands in the Ru(II) heteroleptic complexes. For this, bpy and bathophen coligands were incorporated, creating two unstrained Ru(II) complexes (**9** and **10**), analogous to complex **8** (Table 2). Introduction of the bpy coligands into heteroleptic complex **9** considerably reduced the dark cytotoxicity in comparison to complex **8** and improved the light-mediated potency, with PI = 28. Complex **10**, with bathophen coligands, possessed the same range of activity as **8** under dark conditions, but showed sub-micromolar potency upon irradiation, with PI = 14.

Recently, we discovered that the introduction of a carboxylic acid-contained ligand (2,2′-biquinoline-4,4′-dicarboxylic acid) into Ru(II) complexes reduces the cytotoxicity and produces complexes that can be used for photocaging of small molecules.[62] Therefore, we used the same approach to reduce the cytotoxicity under dark conditions for the complexes **8** and **10**. Accordingly, the chlorine in the pyridyl-pyrazole ligand (type 3) was replaced with a carboxylic acid group and the complexes generated with dmphen (**11**) and bathophen (**12**) coligands. These +1 complexes were studied under dark conditions and possessed up to 15-fold lower cytotoxicity than the corresponding +2 charged complexes **8** and **10** (Figure 4B). Fortunately, incorporation of the carboxylic acid did not affect the light-mediated activity; sub-micromolar potency was exhibited by complex **11** upon irradiation, as the same ligand-deficient Ru(II) active species is produced as for complexes **1**−

https://dx.doi.org/10.1021/acsomega.0c02079
ACS Omega XXXX, XXX, XXX−XXX

8. This modification resulted in the largest phototoxicity index (146) for this group of compounds.

2.6. In-Cell Transcription and Translation Assay. To investigate the impact of the Ru(II) complexes on the essential biological processes, a cell-based transcription and translation assay was performed using the photoconvertible protein, Dendra2, as a reporter for protein synthesis.[75] This allowed for a real-time report in live cells of any damage to the DNA, RNA, or the ribosome or inhibition of any essential components of the cellular machinery responsible for the processes of transcription and translation.

Dendra2 is a photoconvertible protein; upon irradiation, the chromophore within the protein undergoes a chemical reaction and switches from green to red fluorescence, while Dendra2 synthesized after this irradiation step will only show green fluorescence. Therefore, this assay provides a real-time observation of the newly synthesized protein, with ratiometric detection compared to the previously made protein, providing an assay for inhibition of protein synthesis that can be assessed in dose response and with kinetic information. Previously, we established that anticancer 8-hydroxyquinolines (HQs) coordinated with the $[Ru(dmphen)_2]^{2+}$ scaffold exhibit inhibition of protein production at sub-micromolar concentrations, as indicated by the reduction in the expression of Dendra2.[76] Therefore, to narrow down the possible mechanisms of action causing the cytotoxicity, complexes **4** and **8** were tested for inhibition of protein synthesis (Figure 5A,B). Rapamycin was

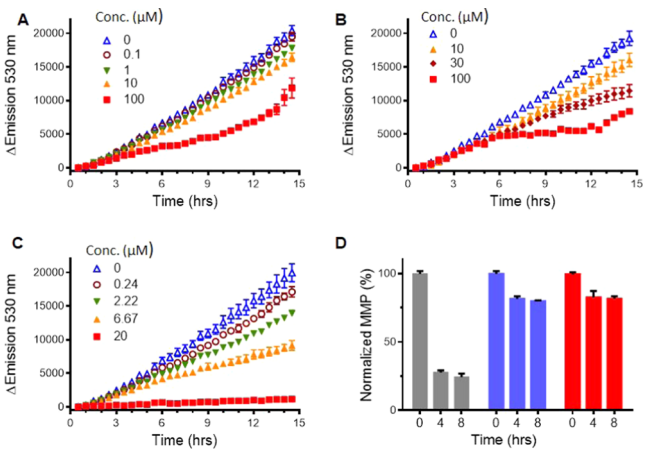

Figure 5. Inhibition of protein synthesis (A–C) and examination of mitochondria dysfunction (D). Emission of the photoconvertible protein, Dendra2, was monitored over time to report on protein production. (A) Complex **4** (0–100 μM); (B) complex **8** (0–100 μM); (C) rapamycin (0–20 μM). (D) Time-dependent inhibition of mitochondrial function with complex **2** upon dark (blue) and light (red) conditions compared with the control compound (carbonyl cyanide *m*-chlorophenyl hydrazone (CCCP), gray).

used as a positive control, with the results shown in Figure 5C. Rapamycin is an inhibitor of the mammalian target of rapamycin (mTOR) pathway, which is involved in regulating protein synthesis. An IC_{50} for inhibition of protein synthesis of 6.3 μM was observed for rapamycin. Complexes **4** and **8** had no effect that resulted in the reduction in Dendra2 production at concentrations up to 30 μM. These data indicate that inhibition of either transcription or translation is not the causative mechanism involved in the cytotoxicity of Ru(II) complexes with pyridyl-pyrazole ligands, in contrast to cytotoxic HQs coordinated with the $[Ru(dmphen)_2]^{2+}$ scaffold.[76]

2.7. Mitochondria Dysfunction. Alternatively, the compounds could cause cell death through damage to the mitochondria. This mechanism of action has been previously established for a variety of anticancer Ru(II) complexes with dmphen coligands.[44,51,55] To test this, the mitochondrial membrane potential was examined by fluorescent dye tetramethylrhodamine ethyl ester perchlorate (TMRE), which is excluded from active mitochondria but not dysfunctional mitochondria. A cyanide compound, carbonyl cyanide *m*-chlorophenyl hydrazone (CCCP), was used as a positive control for mitochondria dysfunction. For this assay, A549 nonsmall cell lung cancer cells were treated with complexes **2**, **4**, and **8**, at concentrations twice their IC_{50} values under both dark and light (1 min with Indigo LED, 29.1 J/cm^2) conditions. The fluorescence intensity from TMRE was normalized, with the no-cells reading set as 0% and the no-treatment cell reading as 100%. Upon treatment of all three compounds, a rapid decrease of 20–30% of the mitochondrial membrane potential was observed (Figure 5D). In contrast, the positive control cyanide compound inhibits ∼80% of the mitochondria function. Thus, the loss of the mitochondrial membrane potential does not appear to be the cause of the cytotoxicity of these complexes.

3. CONCLUSIONS

Previous work using the $[Ru(dmphen)_2]^{2+}$ scaffold resulted in metal complexes that are photoreactive cytotoxins with potential utility for PACT.[17] However, this framework has also shown potential to enhance the anticancer activity of small molecules, such as HQs,[11,76] pyridyl-benzazoles,[16] and modified phenanthrolines.[44,50,55] To expand the repertoire of strained polypyridyl compounds with applications in PACT, we synthesized and investigated the photochemical and biological properties of a group of Ru(II) complexes with pyridyl-pyrazol(in)e ligands. The choice of new five-membered ligands was motivated by the biological potential of the free ligands and previous results for photoactive heteroleptic Ru(II) complexes with pyridyl-benzazole ligands.[16] Recently, we established that the electronic features can be used to tune the photochemistry of Ru(II) complexes for biological applications; this was demonstrated for monodentate ligands, which act as leaving groups.[61,62] Additionally, it is known that Ru(II) complexes that contain the pyridyl-1,2,3-triazole ligand[63] or pyridyl-benzazole ligands[16] are photolabile. Therefore, we hypothesized that pyridyl-pyrazol(in)es can be utilized as bidentate leaving groups for cytotoxic Ru(II) scaffolds. Fortunately, complexes **3**, **4**, **7**, and **8**, which include a phenyl moiety at the 1*N*-position of pyrazol(in)e, exhibited rapid and selective photoejection of the pyrazol(in)e-containing ligand when irradiated with >450 nm light. We established that compounds **1**–**4**, **7**, and **8**, with regular pyridyl-pyrazol(in)e ligands, were at least 20–80-fold more potent than the parent pyridyl-pyrazol(in)es, and exhibited anticancer activity in the HL60 cell line, with IC_{50} values ranging from 0.2 to 7.6 μM. Light activation of **3**, **4**, **7**, and **8** resulted in complete cell death at 10-fold lower concentrations than under dark conditions but did not show a significant improvement in the IC_{50} values. Complexes **5** and **6** with inverse pyridyl-pyrazoline ligands exhibited the same dark potency against the HL60 cell line as **1**–**4**. In addition, these compounds exhibit slow photoejection, which diminishes their utility for PACT. Diversification of the

https://dx.doi.org/10.1021/acsomega.0c02079
ACS Omega XXXX, XXX, XXX–XXX

coligands in the complex improved the phototoxicity indicies from PI = 5 up to 28 for compound **9**. Finally, the introduction of a carboxylic acid in heteroleptic complexes **11** and **12** provided the largest PI values (146 and 59) by a remarkable reduction in the dark cytotoxicity. This points toward a rational design strategy utilizing pendent carboxylic acids for the creation of photoactive heteroleptic Ru (II) complex candidates for PACT.

4. EXPERIMENTAL SECTION

4.1. Materials and Instrumentation. All materials that were purchased from commercial sources were used without any further purification. All ^{1}H NMR were obtained on a Varian mercury spectrometer (400 MHz), and chemical shifts are reported relative to the residual solvent peak of CD_3CN (δ 1.94). Electrospray ionization (ESI) mass spectra were obtained on a Varian 1200L mass spectrometer at the Environmental Research Training Laboratory (ERTL) at the University of Kentucky. The UV/vis absorption spectra were obtained on a BMG Labtech FLUOstar Omega microplate reader. Light activation experiments were performed using a 470 nm LED array from Elixa (for photochemistry and DNA gels) or with >450 nm light using the Indigo LED (for cytotoxicity experiments). The Prism software package was used to analyze the data.

4.2. HPLC Analysis for Purity and Photoejection Products. The purity of each of the Ru(II) complexes **1**−**12** and photoejection products were analyzed using an Agilent 1100 series HPLC equipped with a model G1311A quaternary pump, G1315B UV diode array detector (detection wavelength of 280 nm), and ChemStation software version B.01.03. Chromatographic conditions were optimized on a Column Technologies Inc. A C18 120 Å column was used for compounds **4**, **8**, **10** and **12**, and a Phonomenex Luna 5 μm C18(2) 100 Å was used for compounds **1**−**3**, **6**, **7**, and **11**. Both columns were fitted with a Phenomenex C18 guard column. Mobile phases consisted of 0.1% formic acid in dH_2O and 0.1% formic acid in HPLC grade CH_3CN. The samples of each Ru(II) complex were prepared at a final concentration of 10−100 μM in dH_2O and protected from light (dark controls/purity analysis) or irradiated to determine the photoejection products.

4.3. Synthesis and Characterization of Ru(II) Complexes. *4.3.1. General Procedure for the Synthesis of [Ru(dmphen)$_2$L] Complexes **1**−**8** and **11**.* The starting material $[Ru(dmphen)_2Cl_2]$ (120 mg, 0.2 mmol) and pyrazole-containing ligand (1.1 equiv) were added to 4 mL of ethylene glycol in a 15 mL pressure tube. The mixture was heated at 100−120 °C for 2 h (12 h for compound **1a**) while protected from light. The dark orange solution was allowed to cool to room temperature and poured into 50 mL of dH_2O. Addition of a saturated aq KPF_6 solution (ca. 1 mL) produced a red or red-orange precipitate that was collected by vacuum filtration. The purification of the solid was carried out by flash chromatography (silica gel, loaded in 0.1% KNO_3, 5%H_2O in MeCN). A gradient was run, and the pure complex was eluted at 0.2% KNO_3, 5−10% H_2O in MeCN. The product fractions were concentrated under reduced pressure, and a saturated aq solution of KPF_6 was added, followed by extraction of the complex into CH_2Cl_2. The solvent was removed under reduced pressure to give a solid.

*4.3.1.1. Complex **1**.* Yield: 38 mg (18%). Ratio (%) of diastereomers (Λ)-(*S*)/(Λ)-(*R*) = 1:9. ^{1}H NMR (CD_3CN): δ 8.64−8.69 (m, 1H), 8.51−8.58 (m, 2H), 8.35−8.38 (m, 1H), 8.23−8.27 (m, 1H), 8.04−8.15 (m, 3H), 7.80 (d, *J* = 8.3 Hz, 0.9H), 7.51−7.75 (m, 4.2H), 7.44 (d, *J* = 7.9 Hz, 0.9H), 7.06 (d, *J* = 8.7 Hz, 0.2H), 6.82−6.90 (m, 2.2H), 6.76 (d, *J* = 8.7 Hz, 1.8H), 6.35 (d, *J* = 8.6 Hz, 1.8H), 6.21 (d, *J* = 3.3 Hz, 0.9H), 5.41 (d, *J* = 3.7 Hz, 0.1H), 4.76−4.83 (m, 0.9H), 4.27−4.35 (m, 0.1H), 3.74−3.82 (m, 3.9H), 3.49 (dd, *J* = 17.8, 11.5 Hz, 0.1H), 3.26−3.34 (m, 0.1H), 2.69−2.79 (m, 3.9H), 2.00 (s, 2.7H), 1.96 (s, 0.3H), 1.91 (s, 0.3H), 1.88 (s, 2.7H), 1.85−1.86 (m, 3H). Purity by HPLC = 98% (compound **1a** was detected by HPLC due to oxidation of **1**; less than 2% correspond to contaminants, see Figure S34). ESI MS calcd for $C_{43}H_{39}N_7ORu$ $[M^{2+}\cdot PF_6^-]^+$ 916.19, $[M]^{2+}$ 385.62; found 916.4 $[M^{2+}\cdot PF_6^-]^+$, 385.6 $[M]^{2+}$. UV (CH_3CN): λ_{max} nm ($\varepsilon \times 10^{-3}$) 445 (15.9).

*4.3.1.2. Complex **1a**.* Yield: 95 mg (45%). ^{1}H NMR (CD_3CN): δ 10.70 (brs, 1H), 8.65−8.67 (m, 2H), 8.34 (t, *J* = 8.5 Hz, 2H), 8.24−8.28 (m, 2H), 8.12−8.14 (m, 2H), 7.86 (d, *J* = 7.7 Hz, 1H), 7.73−7.80 (m, 3H), 7.50 (d, *J* = 8.4 Hz, 1H), 7.41 (d, *J* = 8.3 Hz, 1H), 7.02−7.09 (m, 3H), 6.82−6.93 (m, 4H), 3.80 (s, 3H), 2.14 (s, 3H), 1.97 (s, 3H), 1.88 (s, 3H), 1.87 (s, 3H). Purity by HPLC = 99%. ESI MS calcd for $C_{43}H_{37}N_7ORu$ $[M]^{2+}$ 384.61; found 384.5 $[M]^{2+}$. UV (CH_3CN): λ_{max} nm ($\varepsilon \times 10^{-3}$) 435 (12.3).

*4.3.1.3. Complex **2**.* Yield: 73 mg (28%). Ratio (%) of diastereomers (Λ)-(*S*)/(Λ)-(*R*) = 1:3. ^{1}H NMR (CD_3CN): δ 8.64−8.69 (m, 1H), 8.52−8.57 (m, 2H), 8.34−8.38 (m, 1H), 8.22−8.27 (m, 1H), 8.06−8.15 (m, 3H), 7.80 (d, *J* = 8.4 Hz, 0.75H), 7.50−7.75 (m, 5H), 7.44 (d, *J* = 7.8 Hz, 0.75H), 7.31 (d, *J* = 8.5 Hz, 0.5H), 7.24 (d, *J* = 8.4 Hz, 1.5H), 7.13 (d, *J* = 8.4 Hz, 0.5H), 6.83−6.86 (m, 2H), 6.39 (d, *J* = 8.4 Hz, 1H), 6.28 (d, *J* = 4.7 Hz, 0.75H), 5.45 (d, *J* = 4.5 Hz, 0.25H), 4.81−4.88 (m, 0.75H), 4.35−4.42 (m, 0.25H), 3.84 (dd, *J* = 17.9, 12.2 Hz, 0.75H), 3.59 (dd, *J* = 17.6, 11.3 Hz, 0.25H), 3.23−3.31 (m, 0.25H), 2.74−2.82 (m, 1.5H), 2.68 (s, 2.25H), 2.00 (s, 2.25H), 1.91 (s, 0.75H), 1.83−1.89 (m, 6H). Purity by HPLC = 95% (oxidized product was detected; less than 5% correspond to contaminants, see Figure S35). ESI MS calcd for $C_{42}H_{36}ClN_7Ru$ $[M^{2+}\cdot PF_6^-]^+$ 920.14, $[M]^{2+}$ 387.59; found 920.2 $[M^{2+}\cdot PF_6^-]^+$, 387.5 $[M]^{2+}$. UV (CH_3CN): λ_{max} nm ($\varepsilon \times 10^{-3}$) 445 (11.5).

*4.3.1.4. Complex **3**.* Yield: 81 mg (42%). Ratio (%) of diastereomers (Λ)-(*S*)/(Λ)-(*R*) = 9:1. ^{1}H NMR (CD_3CN): δ 8.57−8.63 (m, 1H), 8.46−8.52 (m, 1H), 8.34 (d, *J* = 5.6 Hz, 0.9H), 8.11−8.16 (m, 2H), 7.88−8.03 (m, 3.8H), 7.61−7.82 (m, 5.1H), 7.31−7.39 (m, 2.7H), 7.13−7.21 (m, 0.3H), 7.07 (d, *J* = 8.3 Hz, 0.9H), 6.79−6.92 (m, 3.1H), 6.69 (d, *J* = 8.6 Hz, 0.2H), 6.22−6.39 (m, 1H), 5.86−6.14 (m, 3H), 5.59 (dd, *J* = 12.4, 10.0 Hz, 0.1H), 5.22 (dd, *J* = 15.0, 10.2 Hz, 0.9H), 4.32−4.44 (m, 1H), 3.88 (dd, *J* = 18.1, 10.1 Hz, 0.1H), 3.78 (dd, *J* = 17.8, 15.2 Hz, 0.9H), 3.74 (s, 2.7H), 3.65 (s, 0.3H), 2.91 (s, 0.3H), 2.84 (s, 2.7H), 2.44 (s, 2.7H), 2.40 (s, 0.3H), 1.53−1.54 (m, 5.4H), 1.26−1.28 (m, 0.6H). Purity by HPLC = 98%. ESI MS calcd for $C_{49}H_{43}N_7Ru$ $[M^{2+}\cdot PF_6^-]^+$ 992.22, $[M]^{2+}$ 423.63; found 992.4 $[M^{2+}\cdot PF_6^-]^+$, 423.7 $[M]^{2+}$. UV (CH_3CN): λ_{max} nm ($\varepsilon \times 10^{-3}$) 450 (11.0).

*4.3.1.5. Complex **4**.* Yield: 88 mg (31%). Ratio (%) of diastereomers (Λ)-(*S*)/(Λ)-(*R*) = 3:1. ^{1}H NMR (CD_3CN): δ 8.63 (d, *J* = 8.3 Hz, 0.2H), 8.58 (d, *J* = 8.3 Hz, 0.8H), 8.51 (d, *J* = 8.3 Hz, 0.8H), 8.47 (d, *J* = 8.4 Hz, 0.2H), 8.34−8.36 (m, 1H), 8.13−8.18 (m, 2H), 7.88−8.03 (m, 4H), 7.61−7.81 (m, 5H), 7.31−7.49 (m, 4H), 7.12−7.22 (m, 1H), 7.07 (d, *J* = 8.3 Hz, 0.8H), 6.94−6.98 (m, 0.2H), 6.81−6.84 (m, 1H), 6.26−

https://dx.doi.org/10.1021/acsomega.0c02079
ACS Omega XXXX, XXX, XXX−XXX

6.45 (m, 1H), 5.92−6.20 (m, 3H), 5.63 (dd, J = 12.7, 10.3 Hz, 0.2H), 5.27 (dd, J = 14.8, 10.6 Hz, 0.8H), 4.46 (dd, J = 18.0, 10.7 Hz, 0.8H), 4.40 (dd, J = 18.9, 12.6 Hz, 0.2H), 3.86 (dd, J = 18.9, 10.2 Hz, 0.2H), 3.80 (dd, J = 17.9, 14.7 Hz, 0.8H), 2.91 (s, 0.6H), 2.81 (s, 2.4H), 2.43 (s, 2.4H), 2.37 (s, 0.6H), 1.54 (brs, 4.8H), 1.28 (brs, 1.2H). Purity by HPLC = 96%. ESI MS calcd for $C_{48}H_{40}ClN_7Ru$ $[M^{2+}\cdot PF_6^-]^+$ 996.17, $[M]^{2+}$ 425.61; found 996.2 $[M^{2+}\cdot PF_6^-]^+$, 425.5 $[M]^{2+}$. UV (CH_3CN): λ_{max} nm ($\varepsilon \times 10^{-3}$) 450 (14.9).

4.3.1.6. Complex ***5****.* Yield: 138 mg (56%). Ratio (%) of diastereomers (Λ)-(*S*)/(Λ)-(*R*) = 55:45. ^{1}H NMR (CD_3CN): δ 8.63 (d, J = 8.3 Hz, 0.45H), 8.46−8.54 (m, 2.55H), 8.04−8.19 (m, 2.55H), 7.81−7.97 (m, 2.45H), 7.72−7.75 (m, 1H), 7.60−7.63 (m, 1H), 7.55 (d, J = 8.4 Hz, 0.45H), 7.34−7.49 (m, 2.55H), 7.27−7.29 (m, 1H), 6.84−7.09 (m, 5H), 6.54−6.67 (m, 4H), 6.40−6.46 (m, 1.55H), 6.28 (t, J = 6.2 Hz, 0.45H), 5.49 (dd, J = 11.6, 7.7 Hz, 0.45H), 5.40 (dd, J = 12.2, 8.8 Hz, 0.55H), 3.95 (dd, J = 19.7, 12.2 Hz, 0.45H), 3.77−3.85 (m, 3.55H), 3.33 (s, 1.65H), 3.29 (dd, J = 19.6, 8.7 Hz, 0.55H), 3.19 (dd, J = 19.7, 7.8 Hz, 0.45H), 3.03 (s, 1.35H), 2.10 (s, 1.35H), 2.09 (s, 1.65), 1.87 (s, 1.65H), 1.77 (s, 1.35H), 1.54 (s, 1.35H), 1.41 (s, 1.65H). Purity by HPLC = 95%. ESI MS calcd for $C_{49}H_{43}N_7ORu$ $[M^{2+}\cdot PF_6^-]^+$ 992.22, $[M]^{2+}$ 423.63; found 992.3 $[M^{2+}\cdot PF_6^-]^+$, 423.7 $[M]^{2+}$. UV (CH_3CN): λ_{max} nm ($\varepsilon \times 10^{-3}$) 400 (10.6).

4.3.1.7. Complex ***6****.* Yield: 64 mg (27%). Ratio (%) of diastereomers (Λ)-(*S*)/(Λ)-(*R*) = 3:2. ^{1}H NMR (CD_3CN): δ 8.48−8.63 (m, 3H), 8.06−8.20 (m, 2.6H), 7.83−7.97 (m, 2.4H), 7.72−7.75 (m, 1H), 7.29−7.63 (m, 7H), 6.85−7.11 (m, 3H), 6.29−6.69 (m, 6H), 5.53 (dd, J = 11.7, 8.1 Hz, 0.4H), 5.44 (dd, J = 12.3, 8.9 Hz, 0.6H), 3.99 (dd, J = 19.8, 12.4 Hz, 0.6H), 3.83 (dd, J = 19.7, 11.7 Hz, 0.4H), 3.34 (s, 1.8H), 3.29 (dd, J = 19.8, 9.1 Hz, 0.6H), 3.20 (dd, J = 19.6, 8.1 Hz, 0.4H), 3.00 (s, 1.2H), 2.13 (s, 1.2H), 2.07 (s, 1.8), 1.90 (s, 1.8H), 1.76 (s, 1.2H), 1.55 (s, 1.2H), 1.41 (s, 1.8H). Purity by HPLC = 91%. ESI MS calcd for $C_{48}H_{40}ClN_7Ru$ $[M^{2+}\cdot PF_6^-]^+$ 996.17, $[M]^{2+}$ 425.61; found 996.3 $[M^{2+}\cdot PF_6^-]^+$, 425.6 $[M]^{2+}$. UV (CH_3CN): λ_{max} nm ($\varepsilon \times 10^{-3}$) 400 (12.7).

4.3.1.8. Complex ***7****.* Yield: 44 mg (22%). ^{1}H NMR (CD_3CN): δ 8.47 (d, J = 8.3 Hz, 1H), 8.39 (d, J = 8.3 Hz, 1H), 8.35 (d, J = 8.4 Hz, 1H), 7.99−8.12 (m, 4H), 7.95 (d, J = 8.7 Hz, 1H), 7.84 (td, J = 7.8, 1.3 Hz, 1H), 7.76 (d, J = 8.7 Hz, 1H), 7.65 (d, J = 8.4 Hz, 1H), 7.59 (d, J = 8.3 Hz, 1H), 7.49 (s, 1H), 7.41 (d, J = 8.3 Hz, 1H), 7.32 (d, J = 8.4 Hz, 1H), 7.15−7.16 (m, 1H), 6.95 (d, J = 8.9 Hz, 2H), 6.89 (ddd, J = 8.0, 5.9, 1.5 Hz, 2H), 6.78 (t, J = 7.0 Hz, 1H), 6.71 (d, J = 8.9 Hz, 2H), 6.15 (brs, 1H), 5.40 (brs, 1H), 3.68 (s, 3H), 2.59 (s, 3H), 2.13 (s, 3H), 1.73 (s, 3H), 1.41 (s, 3H). Purity by HPLC = 97%. ESI MS calcd for $C_{49}H_{41}N_7ORu$ $[M^{2+}\cdot PF_6^-]^+$ 990.21, $[M]^{2+}$ 422.62; found 990.2 $[M^{2+}\cdot PF_6^-]^+$, 422.4 $[M]^{2+}$. UV (CH_3CN): λ_{max} nm ($\varepsilon \times 10^{-3}$) 415 (12.8).

4.3.1.9. Complex ***8****.* Yield: 58 mg (30%). ^{1}H NMR (CD_3CN): δ 8.47 (d, J = 8.3 Hz, 1H), 8.40 (d, J = 8.3 Hz, 1H), 8.35 (d, J = 8.4 Hz, 1H), 8.12 (d, J = 7.8 Hz, 1H), 8.04−8.07 (m, 2H), 8.00 (d, J = 8.7 Hz, 1H), 7.95 (d, J = 8.7 Hz, 1H), 7.85 (td, J = 7.8, 1.3 Hz, 1H), 7.76 (d, J = 8.7 Hz, 1H), 7.65 (d, J = 8.4 Hz, 1H), 7.59 (d, J = 8.3 Hz, 1H), 7.56 (s, 1H), 7.41 (d, J = 8.3 Hz, 1H), 7.32 (d, J = 8.4 Hz, 1H), 7.16−7.22 (m, 4H), 6.99 (ddd, J = 8.0, 5.9, 1.5 Hz, 2H), 6.88−6.92 (m, 1H), 6.79−6.82 (m, 2H), 6.16 (brs, 1H), 5.41 (brs, 1H), 2.58 (s, 3H), 2.13 (s, 3H), 1.96 (s, 3H), 1.73 (s, 3H). Purity by HPLC = 95%. ESI MS calcd for $C_{48}H_{38}ClN_7Ru$ $[M^{2+}\cdot PF_6^-]^+$ 994.16, $[M]^{2+}$ 424.60; found 994.1 $[M^{2+}\cdot PF_6^-]^+$, 424.6 $[M]^{2+}$. UV (CH_3CN): λ_{max} nm ($\varepsilon \times 10^{-3}$) 415 (12.2).

4.3.1.10. Complex ***11****.* Yield: 20 mg (20%). ^{1}H NMR (CD_3CN): δ 8.46 (d, J = 8.3 Hz, 1H), 8.39 (d, J = 8.3 Hz, 1H), 8.35 (d, J = 8.4 Hz, 1H), 8.14 (d, J = 7.8 Hz, 1H), 7.99−8.06 (m, 3H), 7.94 (d, J = 8.7 Hz, 1H), 7.85 (t, J = 7.8 Hz, 1H), 7.75 (d, J = 8.6 Hz, 3H), 7.64 (d, J = 8.3 Hz, 1H), 7.62 (s, 1H), 7.59 (d, J = 8.3 Hz, 1H), 7.40 (d, J = 8.3 Hz, 1H), 7.31 (d, J = 8.3 Hz, 1H), 7.17 (d, J = 5.3 Hz, 1H), 7.09 (d, J = 8.0 Hz, 2H), 6.91 (t, J = 7.2 Hz, 1H), 6.78 (t, J = 6.4 Hz, 1H), 6.15 (brs, 1H), 5.40 (brs, 1H), 2.59 (s, 3H), 2.13 (s, 3H), 1.72 (s, 3H), 1.41 (s, 3H). Purity by HPLC = 95%. UV (CH_3CN): λ_{max} nm ($\varepsilon \times 10^{-3}$) 415 (11.1).

4.3.2. General Procedure for Synthesis of Unstrained Ru(II) Complexes ***9****,* ***10*** *and* ***12****.* Starting material [Ru(bpy)$_2$Cl$_2$] (for complex **9**) or [Ru(bathophen)$_2$Cl$_2$] (for complexes **10** and **12**, 0.2 mmol) and the pyridyl-pyrazole ligand (1.1 equiv) were added to 6 mL of EtOH/H_2O mixture (1:1) in a 15 mL pressure tube. The mixture was heated at 90 °C for 2 h. The dark orange solution was allowed to cool to room temperature and poured into 50 mL of dH_2O. Addition of a saturated aq KPF_6 solution (ca. 1 mL) produced a red-orange precipitate that was collected by vacuum filtration. The purification of the solid was carried out by flash chromatography (silica gel, loaded in 0.1% KNO_3, 5%H_2O in MeCN). A gradient was run, and the pure complex was eluted at 0.2% KNO_3, 5−10% H_2O in MeCN. The product fractions were concentrated under reduced pressure, and a saturated aq solution of KPF_6 was added, followed by extraction of the complex into CH_2Cl_2. The solvent was removed under reduced pressure to give a solid.

4.3.2.1. Complex ***9****.* Yield: 122 mg (61%). ^{1}H NMR (CD_3CN): δ 8.42 (d, J = 8.0 Hz, 1H), 8.37 (d, J = 8.2 Hz, 2H), 8.29 (t, J = 7.7 Hz, 2H), 8.03−8.14 (m, 4H), 7.96 (ddd, J = 9.5, 8.0, 1.5 Hz, 1H), 7.86 (d, J = 6.5 Hz, 1H), 7.58−7.65 (m, 3H), 7.46−7.51 (m, 3H), 7.25−7.35 (m, 6H), 7.16−7.20 (m, 2H), 7.12 (d, J = 6.9 Hz, 1H), 7.02−7.08 (m, 2H), 6.87 (ddd, J = 7.2, 5.6, 1.3 Hz, 1H), 6.77 (t, J = 7.1 Hz, 1H), 6.20 (d, J = 7.2 Hz, 1H). Purity by HPLC = 99%. ESI MS calcd for $C_{40}H_{30}ClN_7Ru$ $[M^{2+}\cdot PF_6^-]^+$ 890.09, $[M]^{2+}$ 372.57; found 890.1 $[M^{2+}\cdot PF_6^-]^+$, 372.5 $[M]^{2+}$. UV (CH_3CN): λ_{max} nm ($\varepsilon \times 10^{-3}$) 410 (12.2).

4.3.2.2. Complex ***10****.* Yield: 190 mg (68%). ^{1}H NMR (CD_3CN): δ 8.93 (d, J = 5.4 Hz, 1H), 8.47 (d, J = 5.4 Hz, 1H), 8.40 (d, J = 7.8 Hz, 1H), 8.06−8.21 (m, 4H), 7.99 (d, J = 9.4 Hz, 1H), 7.95 (d, J = 5.4 Hz, 1H), 7.83−7.86 (m, 2H), 7.45−7.76 (m, 25H), 7.16−7.27 (m, 5H), 7.04−7.07 (m, 2H), 6.92 (t, J = 7.5 Hz, 1H), 6.23 (t, J = 7.3 Hz, 1H), 5.77 (d, J = 7.8 Hz, 1H). Purity by HPLC = 98%. ESI MS calcd for $C_{68}H_{46}ClN_7Ru$ $[M^{2+}\cdot PF_6^-]^+$ 1242.22, $[M]^{2+}$ 548.63; found 1242.2 $[M^{2+}\cdot PF_6^-]^+$, 548.6 $[M]^{2+}$. UV (CH_3CN): λ_{max} nm ($\varepsilon \times 10^{-3}$) 425 (23.0).

4.3.2.3. Complex ***12****.* Yield: 160 mg (57%). ^{1}H NMR (CD_3CN): δ 8.94 (d, J = 5.4 Hz, 1H), 8.47 (d, J = 5.4 Hz, 1H), 8.41 (d, J = 7.8 Hz, 1H), 8.07−8.20 (m, 4H), 8.00 (d, J = 9.4 Hz, 1H), 7.95 (d, J = 5.4 Hz, 1H), 7.82−7.86 (m, 4H), 7.45−7.78 (m, 25H), 7.24−7.30 (m, 3H), 7.04−7.08 (m, 2H), 6.94 (t, J = 7.4 Hz, 1H), 6.24 (t, J = 7.3 Hz, 1H), 5.79 (d, J = 7.9 Hz, 1H). Purity by HPLC = 96%. UV (CH_3CN): λ_{max} nm ($\varepsilon \times 10^{-3}$) 425 (24.1).

4.4. Crystallography. Single crystals of compounds **1a**, **4**, and **8** were grown from methylene chloride or acetone by vapor diffusion of diethyl ether, mounted in an inert oil, and

https://dx.doi.org/10.1021/acsomega.0c02079
ACS Omega XXXX, XXX, XXX−XXX

transferred to the cold gas stream of the diffractometer. X-ray diffraction data were collected at 90.0(2) K on either a Nonius KappaCCD diffractometer using Mo$K\alpha$ X-rays or on a Bruker-Nonius X8 Proteum diffractometer with graded-multilayer focused Cu Kα X-rays. Raw data were integrated, scaled, merged, and corrected for Lorentz-polarization effects using either the HKL-SMN package[77] or the APEX2 package.[78] Corrections for absorption were applied using SADABS[79] and XABS2.[80] The structures were solved by SHELXT[81] and refined against F^2 by weighted full-matrix least-squares using SHELXL-2014.[82] For compound **8**, the SQUEEZE routine[83] was used to treat disordered solvent. Hydrogen atoms were placed at the calculated positions and refined using a riding model. Nonhydrogen atoms were refined with the anisotropic displacement parameters. Structures were checked using check CIF tools in Platon[84] and by an R-tensor.[85] Crystal data and relevant details of the structure determinations are summarized below.

*4.4.1. Crystal Data (**1a**, CCDC 2006205).* $C_{47}H_{47}F_{12}N_7O_2P_2Ru$, M_r = 1132.92, monoclinic, $C2/c$, a = 25.3195(5) Å, α = 90°, b = 27.6183(5) Å, β = 116.666(1)°, c = 17.9680(3) Å, γ = 90°, V = 11228.3(4)Å^3, Z = 8, ρ = 1.34 mg/m^3, μ = 3.513 mm^{-1}, $F(000)$ = 4608, crystal size = 0.240 × 0.03 × 0.02 mm^3, θ(max) = 68.450°, 73 439 reflections collected, 10 219 unique reflections (R_{int} = 0.0714), goodness of fit (GOF) = 1.029, R_1 = 0.047 and wR_2 = 0.1305 [$I > 2\sigma(I)$], R_1 = 0.0681 and wR_2 = 0.1442 (all indices), largest difference peak/hole = 1.009/−0.581 e/Å^3.

*4.4.2. Crystal Data (**4**, CCDC 1996034).* $C_{41}H_{40}ClF_{12}N_7P_2Ru$, M_r = 1141.33, triclinic, $P\bar{1}$, a = 10.8291(6) Å, α = 86.860(3)°, b = 11.0247(6) Å, β = 84.770(3)°, c = 21.5477(12) Å, γ = 79.645(2)°, V = 2518.2(2) Å^3, Z = 4, ρ = 1.505 mg/m^3, μ = 4.371 mm^{-1}, $F(000)$ = 1152, crystal size = 0.240 × 0.200 × 0.190 mm^3, θ(max) = 68.460°, 32 007 reflections collected, 8942 unique reflections (R_{int} = 0.0535), GOF = 1.198, R_1 = 0.0598 and wR_2 = 0.1487 [$I > 2\sigma(I)$], R_1 = 0.0620 and wR_2 = 0.1501 (all indices), largest difference peak/hole = 0.999/−0.888 e/Å^3.

*4.4.3. Crystal Data (**8**, CCDC 1996035).* $C_{99}H_{84}Cl_2F_{24}N_{14}O_2P_4Ru_2$, M_r = 2354.72, monoclinic, $C2/c$, a = 28.6521(2) Å, α = 90°, b = 22.6211(2) Å, β = 128.0180(4)°, c = 21.4137(2) Å, γ = 90°, V = 10934.20(17) Å^3, Z = 4, ρ = 1.430 mg/m^3, μ = 0.477 mm^{-1}, $F(000)$ = 4760, crystal size = 0.350 × 0.300 × 0.210 mm^3, θ(max) = 27.697°, 126 391 reflections collected, 12 653 unique reflections (R_{int} = 0.0357), GOF = 1.073, R_1 = 0.0538 and wR_2 = 0.1673 [$I > 2\sigma(I)$], R_1 = 0.0669 and wR_2 = 0.1785 (all indices), largest difference peak/hole = 1.347/−0.677 e/Å^3.

4.5. Counterion Exchange. Compounds **1**−**12** were converted to Cl^- salts by dissolving 5−20 mg of the product in 1−2 mL of methanol. The dissolved product was loaded onto an Amberlite IRA-410 chloride ion exchange column, eluted with methanol, and the solvent was removed in vacuo.

4.6. Photoejection Studies. Quantum yields for the complexes **1**−**8** and **11** with the Cl counterions were determined by an optical approach, as has been described previously.[61] The Ru(II) complexes were analyzed in a 96-well plate at a final concentration of 25−35 μM and a path length of 0.5 cm. Scans were taken at set time points for 300 min. In all cases, the light source was a 470 nm LED array from Elixa. The photon flux of the lamp for irradiation in the plate was determined by a ferrioxalate actinometer (1.77×10^{-8} E/s).

The absorbance of complexes at a concentration of 25−35 μM at 470 nm was from 0.07 to 0.19 with photon absorption probability (F) from 0.14 to 0.36. Therefore, the moles of the photon absorbed have been calculated as the product of photons irradiated and photon absorption probability.

4.7. Cytotoxicity Assay. The HL60 cells were plated at 30 000 cells/well in Opti-MEM media with 1% fetal bovine serum (FBS) and Pen-Strep in 96-well plates. Compounds were serially diluted in opti-MEM with 1% FBS and Pen-Strep in a 96-well plate and then added to the cells. They were then irradiated with 29.1 J/cm^2 light (>450 nm using the Indigo LED) for 1 min or kept in the dark. The cells were incubated with the compounds for 72 h followed by the addition of resazurin. The plates were incubated for 3 h and then read on a SpectraFluor Plus plate reader with an excitation filter of 535 nm and an emission of 595 nm.

4.8. DNA Gel Electrophoresis. Compounds were mixed with 40 μg/mL pUC19 plasmid DNA in 10 mM potassium phosphate buffer, pH 7.4. To determine the effect of light, the samples were irradiated with light (470 nm) from a 200 W light source (LED array from Elixa) for total light doses of 40 J/cm^2. The samples were then incubated for 12 h at room temperature in the dark. Single- and double-strand DNA break controls were prepared, and the DNA samples were resolved on agarose gels, as described previously.[19] In brief, the samples were resolved on a 1% agarose gel prepared in tris-acetate buffer with 0.3 μg of plasmid/lane. The gels were stained with 0.5 μg/mL ethidium bromide in Tris-acetate buffer at room temperature for 40 min, destained with tris-acetate buffer, and imaged on a ChemiDoc MP system (Bio-Rad).

4.9. Dendra2 Transcription−Translation Assay. 96-well plates were coated with matrigel followed by the addition of HEK T-Rex cells at a density of 30 000 cells/well and incubated with 1 μg/mL of tetracycline for 16 h. The media was removed and 50 μL of L-15 media containing 1 μg/mL tetracycline along with compound was added to each well and allowed to incubate for 1 h. The plates were then illuminated with a 405 nm LED flood array for 1 min and then read in kinetic mode on a SpectraFluor Plus (Tecan) set to 37 °C. The plates were read every 30 min for 15 h with excitation and emission wavelengths of 480 and 530 nm for newly translated Dendra2 and 535 and 595 nm for post-translated Dendra2.[75]

■ ASSOCIATED CONTENT

Supporting Information

The Supporting Information is available free of charge at https://pubs.acs.org/doi/10.1021/acsomega.0c02079.

Additional schemes and figures for synthetic methods, characterization, photochemical and photobiological analyses (PDF)

■ AUTHOR INFORMATION

Corresponding Authors

Dmytro Havrylyuk − *Department of Chemistry, University of Kentucky, Lexington, Kentucky 40506, United States;* orcid.org/0000-0001-7766-9923; Email: dyha223@uky.edu

Edith C. Glazer − *Department of Chemistry, University of Kentucky, Lexington, Kentucky 40506, United States;* orcid.org/0000-0002-0190-7742; Email: ec.glazer@uky.edu

https://dx.doi.org/10.1021/acsomega.0c02079
ACS Omega XXXX, XXX, XXX−XXX

Authors

David K. Heidary − *Department of Chemistry, University of Kentucky, Lexington, Kentucky 40506, United States*

Yang Sun − *Department of Chemistry, University of Kentucky, Lexington, Kentucky 40506, United States*

Sean Parkin − *Department of Chemistry, University of Kentucky, Lexington, Kentucky 40506, United States*

Complete contact information is available at: https://pubs.acs.org/10.1021/acsomega.0c02079

Author Contributions

The manuscript was written through the contributions of all authors. All authors have given approval to the final version of the manuscript.

Notes

The authors declare no competing financial interest.

■ ACKNOWLEDGMENTS

We gratefully acknowledge the National Institutes of Health (grant GM107586) for the support of this research. Crystallographic work was made possible by the National Science Foundation (NSF) MRI program, grants CHE-0319176 and CHE-1625732.

■ REFERENCES

(1) Furrer, J.; Süss-Fink, G. Thiolato-bridged Dinuclear Arene Ruthenium Complexes and Their Potential as Anticancer Drugs. *Coord. Chem. Rev.* **2016**, *309*, 36−50.

(2) Mari, C.; Pierroz, V.; Ferrari, S.; Gasser, G. Combination of Ru(II) Complexes and Light: New Frontiers in Cancer Therapy. *Chem. Sci.* **2015**, *6*, 2660−2686.

(3) Bergamo, A.; Gaiddon, C.; Schellens, J. H.; Beijnen, J. H.; Sava, G. Approaching Tumour Therapy Beyond Platinum Drugs: Status of the Art and Perspectives of Ruthenium Drug Candidates. *J. Inorg. Biochem.* **2012**, *106*, 90−99.

(4) Salassa, L. Polypyridyl Metal Complexes with Biological Activity. *Eur. J. Inorg. Chem.* **2011**, *2011*, 4931−4947.

(5) Zeng, L.; Gupta, P.; Chen, Y.; Wang, E.; Ji, L.; Chao, H.; Chen, Z. S. The Development of Anticancer Ruthenium(II) Complexes: from Single Molecule Compounds to Nanomaterials. *Chem. Soc. Rev.* **2017**, *46*, 5771−5804.

(6) Notaro, A.; Gasser, G. Monomeric and Dimeric Coordinatively Saturated and Substitutionally Inert Ru(II) Polypyridyl Complexes as Anticancer Drug Candidates. *Chem. Soc. Rev.* **2017**, *46*, 7317−7337.

(7) Rademaker-Lakhai, J. M.; van den Bongard, D.; Pluim, D.; Beijnen, J. H.; Schellens, J. H. A Phase I and Pharmacological Study with Imidazolium-trans-DMSO-imidazole-tetrachlororuthenate, a Novel Ruthenium Anticancer Agent. *Clin. Cancer Res.* **2004**, *10*, 3717−3727.

(8) Trondl, R.; Heffeter, P.; Kowol, C. R.; Jakupec, M. A.; Berger, W.; Keppler, B. K. NKP-1339, the First Ruthenium-based Anticancer Drug on the Edge to Clinical Application. *Chem. Sci.* **2014**, *5*, 2925−2932.

(9) Weiss, A.; Berndsen, R. H.; Dubois, M.; Muller, C.; Schibli, R.; Griffioen, A. W.; Dyson, P. J.; Nowak-Sliwinska, P. In Vivo Anti-tumor Activity of the Organometallic Ruthenium(II)-arene Complex [Ru(η6-p-cymene)Cl2(pta)] (RAPTA-C) in Human Ovarian and Colorectal Carcinomas. *Chem. Sci.* **2014**, *5*, 4742−4748.

(10) Ang, W. H.; Casini, A.; Sava, G.; Dyson, P. J. Organometallic Ruthenium-based Antitumor Compounds with Novel Modes of Action. *J. Organomet. Chem.* **2011**, *696*, 989−998.

(11) Heidary, D. K.; Howerton, B. S.; Glazer, E. C. Coordination of Hydroxyquinolines to a Ruthenium Bis-dimethyl-phenanthroline Scaffold Radically Improves Potency for Potential as Antineoplastic Agents. *J. Med. Chem.* **2014**, *57*, 8936−8946.

(12) Pierroz, V.; Joshi, T.; Leonidova, A.; Mari, C.; Schur, J.; Ott, I.; Spiccia, L.; Ferrari, S.; Gasser, G. Molecular and Cellular Characterization of the Biological Effects of Ruthenium(II) Complexes Incorporating 2-Pyridyl-2-pyrimidine-4-carboxylic Acid. *J. Am. Chem. Soc.* **2012**, *134*, 20376−20387.

(13) Notaro, A.; Jakubaszek, M.; Rotthowe, N.; Maschietto, F.; Vinck, R.; Felder, P. S.; Goud, B.; Tharaud, M.; Ciofini, I.; Bedioui, F.; Winter, R. F.; Gasser, G. Increasing the Cytotoxicity of Ru(II) Polypyridyl Complexes by tuning the Electronic Structure of Dioxo Ligands. *J. Am. Chem. Soc.* **2020**, *142*, 6066−6084.

(14) Howerton, B. S.; Heidary, D. K.; Glazer, E. C. Strained Ruthenium Complexes Are Potent Light-activated Anticancer Agents. *J. Am. Chem. Soc.* **2012**, *134*, 8324−8327.

(15) Albani, B. A.; Pena, B.; Leed, N. A.; de Paula, N. A.; Pavani, C.; Baptista, M. S.; Dunbar, K. R.; Turro, C. Marked Improvement in Photoinduced Cell Death by a New Tris-heteroleptic Complex with Dual Action: Singlet Oxygen Sensitization and Ligand Dissociation. *J. Am. Chem. Soc.* **2014**, *136*, 17095−17101.

(16) Havrylyuk, D.; Heidary, D. K.; Nease, L.; Parkin, S.; Glazer, E. C. Photochemical Properties and Structure−Activity Relationships of RuII Complexes with Pyridylbenzazole Ligands as Promising Anticancer Agents. *Eur. J. Inorg. Chem.* **2017**, *2017*, 1687−1694.

(17) Hidayatullah, A. N.; Wachter, E.; Heidary, D. K.; Parkin, S.; Glazer, E. C. Photoactive Ru(II) Complexes With Dioxinophenanthroline Ligands Are Potent Cytotoxic Agents. *Inorg. Chem.* **2014**, *53*, 10030−10032.

(18) Wachter, E.; Glazer, E. C. Mechanistic Study on the Photochemical "Light Switch" Behavior of $[Ru(bpy)_2dmdppz]^{2+}$. *J. Phys. Chem. A* **2014**, *118*, 10474−10486.

(19) Wachter, E.; Heidary, D. K.; Howerton, B. S.; Parkin, S.; Glazer, E. C. Light-Activated Ruthenium Complexes Photobind DNA and are Cytotoxic in the Photodynamic Therapy Window. *Chem. Commun.* **2012**, *48*, 9649−9651.

(20) Wachter, E.; Howerton, B. S.; Hall, E. C.; Parkin, S.; Glazer, E. C. A New Type of DNA "Light-Switch": a Dual Photochemical Sensor and Metalating Agent for Duplex and G-quadruplex DNA. *Chem. Commun.* **2014**, *50*, 311−313.

(21) Kohler, L.; Nease, L.; Vo, P.; Garofolo, J.; Heidary, D. K.; Thummel, R. P.; Glazer, E. C. Photochemical and Photobiological Activity of Ru(II) Homoleptic and Heteroleptic Complexes Containing Methylated Bipyridyl-type Ligands. *Inorg. Chem.* **2017**, *56*, 12214−12223.

(22) Roque, J., III; Havrylyuk, D.; Barrett, P. C.; Sainuddin, T.; McCain, J.; Colón, K.; Sparks, W. T.; Bradner, E.; Monro, S.; Heidary, D.; Cameron, C. G.; Glazer, E. C.; McFarland, S. A. Strained, Photoejecting Ru(II) Complexes that are Cytotoxic Under Hypoxic Conditions. *Photochem. Photobiol.* **2020**, *96*, 327−339.

(23) Cuello-Garibo, J.-A.; Meijer, M. S.; Bonnet, S. To Cage or to Be Caged? The Cytotoxic Species in Ruthenium-Based Photoactivated Chemotherapy Is not Always the Metal. *Chem. Commun.* **2017**, *53*, 6768−6771.

(24) Chan, H.; Ghrayche, J. B.; Wei, J.; Renfrew, A. K. Photolabile Ruthenium(II)-Purine Complexes: Phototoxicity, DNA Binding, and Light-Triggered Drug Release. *Eur. J. Inorg. Chem.* **2017**, *2017*, 1679−1686.

(25) Perez-Fernandez, R.; Goya, P.; Elguero, J. A Review of Recent Progress (2002-2012) on the Biological Activities of Pyrazoles. *ARKIVOC* **2014**, *2*, 233−293.

(26) Arber, N.; Eagle, C. J.; Spicak, J.; Racz, I.; Dite, P.; Hajer, J.; Zavoral, M.; Lechuga, M. J.; Gerletti, P.; Tang, J.; Rosenstein, R. B.; Macdonald, K.; Bhadra, P.; Fowler, R.; Wittes, J.; Zauber, A. G.; Solomon, S. D.; Levin, B. Celecoxib for the Prevention of Colorectal Adenomatous Polyps. *New Engl. J. Med.* **2006**, *355*, 885−895.

(27) https://www.fda.gov/drugs/resources-information-approved-drugs/fda-approves-encorafenib-and-binimetinib-combination-unresectable-or-metastatic-melanoma-braf.

(28) Qin, Y. J.; Li, Y. J.; Jiang, A. Q.; Yang, M. R.; Zhu, Q. Z.; Dong, H.; Zhu, H. L. Design, Synthesis and Biological Evaluation of Novel

https://dx.doi.org/10.1021/acsomega.0c02079
ACS Omega XXXX, XXX, XXX−XXX

Pyrazoline-containing Derivatives as Potential Tubulin Assembling Inhibitors. *Eur. J. Med. Chem.* **2015**, *94*, 447−457.
(29) Raghav, N.; Singh, M. SAR Studies of Differently Functionalized Chalcones Based Hydrazones and Their Cyclized Derivatives as Inhibitors of Mammalian Cathepsin B and Cathepsin H. *Bioorg. Med. Chem.* **2014**, *22*, 4233−4245.
(30) Shuck, S. C.; Turchi, J. J. Targeted Inhibition of Replication Protein A Reveals Cytotoxic Activity, Synergy with Chemotherapeutic DNA-damaging Agents, and Insight into Cellular Function. *Cancer Res.* **2010**, *70*, 3189−3198.
(31) Havrylyuk, D.; Kovach, N.; Zimenkovsky, B.; Vasylenko, O.; Lesyk, R. Synthesis and Anticancer Activity of Isatin-based Pyrazolines and Thiazolidines Conjugates. *Arch. Pharm.* **2011**, *344*, 514−522.
(32) Havrylyuk, D.; Zimenkovsky, B.; Vasylenko, O.; Day, C. W.; Smee, D. F.; Grellier, P.; Lesyk, R. Synthesis and Biological Activity Evaluation of 5-pyrazoline Substituted 4-thiazolidinones. *Eur. J. Med. Chem.* **2013**, *66*, 228−237.
(33) Havrylyuk, D.; Zimenkovsky, B.; Vasylenko, O.; Gzella, A.; Lesyk, R. Synthesis of New 4-thiazolidinone-, Pyrazoline-, and Isatin-based Conjugates with Promising Antitumor Activity. *J. Med. Chem.* **2012**, *55*, 8630−8641.
(34) Havrylyuk, D.; Zimenkovsky, B.; Vasylenko, O.; Zaprutko, L.; Gzella, A.; Lesyk, R. Synthesis of Novel Thiazolone-based Compounds Containing Pyrazoline Moiety and Evaluation of Their Anticancer Activity. *Eur. J. Med. Chem.* **2009**, *44*, 1396−1404.
(35) Havrylyuk, D.; Roman, O.; Lesyk, R. Synthetic Approaches, Structure Activity Relationship and Biological Applications for Pharmacologically Attractive Pyrazole/pyrazoline-thiazolidine-based Hybrids. *Eur. J. Med. Chem.* **2016**, *113*, 145−166.
(36) Avdieiev, S.; Gera, L.; Havrylyuk, D.; Hodges, R. S.; Lesyk, R.; Ribrag, V.; Vassetzky, Y.; Kavsan, V. Bradykinin Antagonists and Thiazolidinone derivatives as New Potential Anti-cancer Compounds. *Bioorg. Med. Chem.* **2014**, *22*, 3815−3823.
(37) Havrylyuk, D.; Zimenkovsky, B.; Karpenko, O.; Grellier, P.; Lesyk, R. Synthesis of Pyrazoline-thiazolidinone Hybrids with Trypanocidal Activity. *Eur. J. Med. Chem.* **2014**, *85*, 245−254.
(38) Budzisz, E.; Miernicka, M.; Lorenz, I.-P.; Mayer, P.; Krajewska, U.; Rozalski, M. Synthesis and X-ray Structure of Platinum(II), Palladium(II) and Copper(II) Complexes with Pyridine-pyrazole Ligands: Influence of Ligands' Structure on Cytotoxic Activity. *Polyhedron* **2009**, *28*, 637−645.
(39) Kupcewicz, B.; Ciolkowski, M.; Karwowski, B. T.; Rozalski, M.; Krajewska, U.; Lorenz, I.-P.; Mayer, P.; Budzisz, E. Copper(II) Complexes with Pyrazole Derivatives − Synthesis, Crystal Structure, DFT Calculations and Cytotoxic Activity. *J. Mol. Struct.* **2013**, *1052*, 32−37.
(40) Wang, S.; Shao, W.; Li, H.; Liu, C.; Wang, K.; Zhang, J. Synthesis, Characterization and Cytotoxicity of the Gold(III) Complexes of 4,5-dihydropyrazole-1-carbothioamide Derivatives. *Eur. J. Med. Chem.* **2011**, *46*, 1914−1918.
(41) Huang, Y. C.; Haribabu, J.; Chien, C. M.; Sabapathi, G.; Chou, C. K.; Karvembu, R.; Venuvanalingam, P.; Ching, W. M.; Tsai, M. L.; Hsu, S. C. N. Half-sandwich Ru(η(6)-p-cymene) Complexes Featuring Pyrazole Appended Ligands: Synthesis, DNA Binding and in vitro Cytotoxicity. *J. Inorg. Biochem.* **2019**, *194*, 74−84.
(42) Yang, G. W.; Zhang, X.; Li, G. M.; Yang, J.; Shen, L.; Chen, D. Y.; Li, Q. Y.; Zou, D. F. Photochemical Property of a Ru(II) Compound Based on 3-(2-pyridyl)pyrazole and 2,2'-bipyridine for Ablation of Cancer Cells. *New J. Chem.* **2018**, *42*, 5395−5402.
(43) Thota, S.; Imran, M.; Udugula, M.; Yerra, R.; Karki, S. S.; Balzarini, J.; De Clercq, E. Synthesis, Spectroscopic Characterization and in vitro Antitumor Activities of Some Novel Mononuclear Ru(II) Complexes. *Chin. Chem. Lett.* **2012**, *23*, 466−469.
(44) Tang, B.; Wan, D.; Lai, S.-H.; Yang, H.-H.; Zhang, C.; Wang, X.-Z.; Zeng, C.-C.; Liu, Y.-J. Design, Synthesis and Evaluation of Anticancer Activity of Ruthenium (II) Polypyridyl Complexes. *J. Inorg. Biochem.* **2017**, *173*, 93−104.
(45) Huang, H.-L.; Li, Z.-Z.; Liang, Z.-H.; Liu, Y.-J. Cell Cycle Arrest, Cytotoxicity, Apoptosis, DNA-Binding, Photocleavage, and Antioxidant Activity of Octahedral Ruthenium(II) Complexes. *Eur. J. Inorg. Chem.* **2011**, *2011*, 5538−5547.
(46) Lai, S.-H.; Jiang, G.-B.; Yao, J.-H.; Li, W.; Han, B.-J.; Zhang, C.; Zeng, C.-C.; Liu, Y.-J. Cytotoxic Activity, DNA Damage, Cellular Uptake, Apoptosis and Western Blot Analysis of Ruthenium(II) Polypyridyl Complex Against Human Lung Decarcinoma A549 Cell. *J. Inorg. Biochem.* **2015**, *152*, 1−9.
(47) Liang, Z.-H.; Li, Z.-Z.; Huang, H.-L.; Liu, Y.-J. Ruthenium(II) Complexes: Synthesis, Cytotoxicity in vitro, Apoptosis, DNA-binding, Photocleavage, and Antioxidant Activity Studies. *J. Coord. Chem.* **2011**, *64*, 3342−3352.
(48) Lin, G.-J.; Jiang, G.-B.; Xie, Y.-Y.; Huang, H.-L.; Liang, Z.-H.; Liu, Y.-J. Cytotoxicity, Apoptosis, Cell Cycle Arrest, Reactive Oxygen Species, Mitochondrial Membrane Potential, and Western Blotting Analysis of Ruthenium(II) Complexes. *JBIC, J. Biol. Inorg. Chem.* **2013**, *18*, 873−882.
(49) Liu, Y.-J.; Zeng, C.-H.; Yao, J.-H.; Wu, F.-H.; He, L.-X.; Huang, H.-L. Synthesis, Structure, DNA-Binding Properties, and Cytotoxicity of Ruthenium(II) Polypyridyl Complexes. *Chem. Biodiversity* **2010**, *7*, 1770−1783.
(50) Wan, D.; Lai, S.-H.; Zeng, C.-C.; Zhang, C.; Tang, B.; Liu, Y.-J. Ruthenium(II) Polypyridyl Complexes: Synthesis, Characterization and Anticancer Activity Studies on BEL-7402 Cells. *J. Inorg. Biochem.* **2017**, *173*, 1−11.
(51) Wan, D.; Tang, B.; Wang, Y.-J.; Guo, B.-H.; Yin, H.; Yi, Q.-Y.; Liu, Y.-J. Synthesis and Anticancer Properties of Ruthenium (II) Complexes as Potent Apoptosis Inducers Through Mitochondrial Disruption. *Eur. J. Med. Chem.* **2017**, *139*, 180−190.
(52) Wang, J.-Q.; Zhao, Z.-Z.; Bo, H.-B.; Chen, Q.-Z. Synthesis, Characterization, and Antitumor Properties of Ruthenium(II) Anthraquinone Complexes. *J. Coord. Chem.* **2016**, *69*, 177−189.
(53) Xie, Y.-Y.; Jiang, G.-B.; Yao, J.-H.; Lin, G.-J.; Huang, H.-L.; Wang, X.-Z.; Liu, Y.-J. DNA-binding, Antioxidant activity, and Bbioactivity Studies of Ruthenium(II) Complexes Containing Amino Substituents. *J. Coord. Chem.* **2013**, *66*, 2423−2433.
(54) Xie, Y.-Y.; Li, Z.-Z.; Lin, G.-J.; Huang, H.-L.; Wang, X.-Z.; Liang, Z.-H.; Jiang, G.-B.; Liu, Y.-J. DNA Interaction, Cytotoxicity, Apoptotic Activity, Cell Cycle Arrest, Reactive Oxygen Species and Mitochondrial Membrane Potential Assay Induced by Ruthenium(II) Polypyridyl Complexes. *Inorg. Chim. Acta* **2013**, *405*, 228−234.
(55) Zeng, C.-C.; Lai, S.-H.; Yao, J.-H.; Zhang, C.; Yin, H.; Li, W.; Han, B.-J.; Liu, Y.-J. The Induction of Apoptosis in HepG-2 Cells by Ruthenium(II) Complexes Through an Intrinsic ROS-mediated Mitochondrial Dysfunction Pathway. *Eur. J. Med. Chem.* **2016**, *122*, 118−126.
(56) Zeng, C.-H.; Liu, Y.-J.; Li, Z.-Z.; Liang, Z.-H.; Huang, H.-L.; Wu, F.-H. DNA-binding, Antioxidant Activity and in vitro Cytotoxicity Induced by Ruthenium(II) Complexes Containing Polypyridyl Ligands. *Transition Met. Chem.* **2010**, *35*, 731−736.
(57) Zhang, C.; Han, B.-J.; Zeng, C.-C.; Lai, S.-H.; Li, W.; Tang, B.; Wan, D.; Jiang, G.-B.; Liu, Y.-J. Synthesis, Characterization, in vitro Cytotoxicity and Anticancer Effects of Ruthenium (II) Complexes on BEL-7402 Cells. *J. Inorg. Biochem.* **2016**, *157*, 62−72.
(58) Zhang, C.; Zeng, C.-C.; Lai, S.-H.; Xing, D.-G.; Li, W.; Han, B.-J.; Liu, Y.-J. Synthesis, Cytotoxicity in vitro, Apoptosis, Cell Cycle Arrest and Comet Assay of Asymmetry Ruthenium(II) Complexes. *Polyhedron* **2016**, *106*, 115−124.
(59) Guo, Q.-F.; Liu, S.-H.; Liu, Q.-H.; Xu, H.-H.; Zhao, J.-H.; Wu, H.-F.; Li, X.-Y.; Wang, J.-W. Synthesis, Characterization, Photocleavage, Cytotoxicity in vitro, Apoptosis, and Cell Cycle Arrest of Ruthenium(II) Complexes. *J. Coord. Chem.* **2012**, *65*, 1781−1791.
(60) Glazer, E. C.; Heidary, D. K. Light-Activated Compounds. US9290528B1, 2016.
(61) Havrylyuk, D.; Deshpande, M.; Parkin, S.; Glazer, E. C. Ru(II) Complexes with Diazine Ligands: Electronic Modulation of the Coordinating Group Is Key to the Design of "Dual Action" Photoactivated Agents. *Chem. Commun.* **2018**, *54*, 12487−12490.

https://dx.doi.org/10.1021/acsomega.0c02079
ACS Omega XXXX, XXX, XXX−XXX

(62) Havrylyuk, D.; Stevens, K.; Parkin, S.; Glazer, E. C. Toward Optimal Ru(II) Photocages: Balancing Photochemistry, Stability, and Biocompatibility Through Fine Tuning of Steric, Electronic, and Physiochemical Features. *Inorg. Chem.* **2020**, *59*, 1006−1013.
(63) Lo, W. K. C.; Huff, G. S.; Cubanski, J. R.; Kennedy, A. D. W.; McAdam, C. J.; McMorran, D. A.; Gordon, K. C.; Crowley, J. D. Comparison of Inverse and Regular 2-Pyridyl-1,2,3-triazole "Click" Complexes: Structures, Stability, Electrochemical, and Photophysical Properties. *Inorg. Chem.* **2015**, *54*, 1572−1587.
(64) Scattergood, P. A.; Khushnood, U.; Tariq, A.; Cooke, D. J.; Rice, C. R.; Elliott, P. I. P. Photochemistry of $[Ru(pytz)(btz)_2]^{2+}$ and Characterization of a κ1-btz Ligand-Loss Intermediate. *Inorg. Chem.* **2016**, *55*, 7787−7796.
(65) Mamolo, M. G.; Zampieri, D.; Falagiani, V.; Vio, L.; Banfi, E. Synthesis and Antimycobacterial Activity of 5-aryl-1-isonicotinoyl-3-(pyridin-2-yl)-4,5-dihydro-1H-pyrazole Derivatives. *Il Farmaco* **2001**, *56*, 593−599.
(66) Rurack, K.; Bricks, J. L. Towards Simple and Efficient Molecular Reporters: Combining Electron Transfer and Charge Transfer in Functional Dyes of Donor-acceptor-spacer-donor Constitution. *ARKIVOC* **2001**, *11*, 31−40.
(67) Li, X.; Wang, L.; Long, L.; Xiao, J.; Hu, Y.; Li, S. Synthesis and Biological Evaluation of 1,2,4-trisubstituted Imidazoles and 1,3,5-trisubstituted Pyrazoles as Inhibitors of Transforming Growth Factor β Type 1 Receptor (ALK5). *Bioorg. Med. Chem. Lett.* **2009**, *19*, 4868−4872.
(68) Gong, Z.-L.; Ge, F.; Zhao, B.-X. Novel Pyrazoline-based Selective Fluorescent Sensor for Zn^{2+} in Aqueous Media. *Sens. Actuators, B* **2011**, *159*, 148−153.
(69) Wang, P.; Onozawa-Komatsuzaki, N.; Katoh, R.; Himeda, Y.; Sugihara, H.; Arakawa, H.; Kasuga, K. Structure and Properties of Diastereoisomers of a Ruthenium(II) Complex Having a Pyridylpyrazoline Derivative as a Ligand. *Chem. Lett.* **2001**, *30*, 940−941.
(70) Rillema, D. P.; Jones, D. S. Structure of Tris(2,2'-bipyridyl)-ruthenium(II) Hexafluorophosphate, $[Ru(bipy)_3][PF_6]_2$; X-ray Crystallographic Determination. *J. Chem. Soc., Chem. Commun.* **1979**, *19*, 849−851.
(71) Greguric, A.; Greguric, I. D.; Hambley, T. W.; Aldrich-Wright, J. R.; Collins, J. G. Minor Groove Intercalation of Δ-$[Ru(Me_2phen)_2dppz]^{2+}$ to the Hexanucleotide $d(GTCGAC)_2$. *J. Chem. Soc., Dalton Trans.* **2002**, 849−855.
(72) Ashby, M. T.; Alguindigue, S. S.; Khan, M. A. Kinetic Element Effect for Atropisomerization of an Organometallic Complex of the Misdirected Ligand 1,1'-Biisoquinoline. *Organometallics* **2000**, *19*, 547−552.
(73) Azar, D. F.; Audi, H.; Farhat, S.; El-Sibai, M.; Abi-Habib, R. J.; Khnayzer, R. S. Phototoxicity of Strained Ru(II) Complexes: Is it the Metal Complex or the Dissociating Ligand? *Dalton Trans.* **2017**, *46*, 11529−11532.
(74) Collin, J. P.; Sauvage, J. P. Synthesis and Study of Mononuclear Ruthenium(II) Complexes of Sterically Hindering Diimine Chelates. Implications for the Catalytic Oxidation of Water to Molecular Oxygen. *Inorg. Chem.* **1986**, *25*, 135−141.
(75) Heidary, D. K.; Fox, A.; Richards, C. I.; Glazer, E. C. A High-Throughput Screening Assay Using a Photoconvertable Protein for Identifying Inhibitors of Transcription, Translation, or Proteasomal Degradation. *SLAS Discovery* **2017**, *22*, 399−407.
(76) Havrylyuk, D.; Howerton, B. S.; Nease, L.; Parkin, S.; Heidary, D. K.; Glazer, E. C. Structure-activity Relationships of Anticancer Ruthenium(II) Complexes with Substituted Hydroxyquinolines. *Eur. J. Med. Chem.* **2018**, *156*, 790−799.
(77) Otwinowski, Z.; Minor, W. Processing of X-ray Diffraction Data Collected in Oscillation Mode. *Methods Enzymol.* **1997**, *276*, 307−326.
(78) APEX2. *Programs for Data Collection and Data Reduction*; Bruker-Nonius: Madison, WI.
(79) Krause, L.; Herbst-Irmer, R.; Sheldrick, G. M.; Stalke, D. Comparison of Silver and Molybdenum Microfocus X-ray Sources for Single-crystal Structure Determination. *J. Appl. Crystallogr.* **2015**, *48*, 3−10.
(80) Parkin, S.; Moezzi, B.; Hope, H. XABS2: an Empirical Absorption Correction Program. *J. Appl. Crystallogr.* **1995**, *28*, 53−56.
(81) Sheldrick, G. M. SHELXT − Integrated Space-group and Crystal-structure Determination. *Acta Crystallogr., Sect. A: Found. Adv.* **2015**, *71*, 3−8.
(82) Sheldrick, G. M. Structure Determination Revisited. *Acta Crystallogr., Sect. A: Found. Adv.* **2015**, *71*, S9.
(83) van der Sluis, P.; Spek, A. L. BYPASS: an Effective Method for the Refinement of Crystal Structures Containing Disordered Solvent Regions. *Acta Crystallogr., Sect. A: Found. Crystallogr.* **1990**, *46*, 194−201.
(84) Spek, A. L. Structure Validation in Chemical Crystallography. *Acta Crystallogr., Sect. D: Biol. Crystallogr.* **2009**, *65*, 148−155.
(85) Parkin, S. Expansion of Scalar Validation Criteria to Three Dimensions: the R Tensor. *Acta Crystallogr., Sect. A: Found. Crystallogr.* **2000**, *56*, 157−162.

https://dx.doi.org/10.1021/acsomega.0c02079
ACS Omega XXXX, XXX, XXX−XXX